Hearing Research 330 (2015) 62–77

Contents lists available at ScienceDirect

Hearing Research

journal homepage: www.elsevier.com/locate/heares

Comparative gene expression study of the vestibular organ of the *Igf1* deficient mouse using whole-transcript arrays

Lourdes Rodríguez-de la Rosa [a, b, c], Hortensia Sánchez-Calderón [a], Julio Contreras [a, b, d], Silvia Murillo-Cuesta [a, b, c], Sandra Falagan [e], Carlos Avendaño [c, e], Joaquín Dopazo [b, f], Isabel Varela-Nieto [a, b, c, 1], Marta Milo [g, *, 1]

[a] *Neurobiology of Hearing, Department of Endocrine and Nervous System Pathophysiology, Alberto Sols Biomedical Research Institute (IIBM), CSIC-UAM, Madrid, Spain*
[b] *Biomedical Research Networking Center on Rare Diseases (CIBERER), Institute of Health Carlos III (ISCIII), Madrid, Spain*
[c] *IdiPAZ Institute for Health Research, Madrid, Spain*
[d] *Department of Anatomy, Faculty of Veterinary, Complutense University, Madrid, Spain*
[e] *Department of Anatomy, Faculty of Medicine, Autonomous University, Madrid, Spain*
[f] *Department of Computational Genomics, Centro de Investigación Príncipe Felipe, Valencia, Spain*
[g] *Department of Biomedical Science, University of Sheffield, Sheffield, UK*

ARTICLE INFO

Article history:
Received 10 March 2015
Received in revised form
27 August 2015
Accepted 28 August 2015
Available online 1 September 2015

Keywords:
Insulin like growth factor 1
mRNAs
Transcriptomics
Affymetrix mouse gene 1.1. ST arrays

ABSTRACT

The auditory and vestibular organs form the inner ear and have a common developmental origin. Insulin like growth factor 1 (IGF-1) has a central role in the development of the cochlea and maintenance of hearing. Its deficiency causes sensorineural hearing loss in man and mice. During chicken early development, IGF-1 modulates neurogenesis of the cochleovestibular ganglion but no further studies have been conducted to explore the potential role of IGF-1 in the vestibular system. In this study we have compared the whole transcriptome of the vestibular organ from wild type and *Igf1*$^{-/-}$ mice at different developmental and postnatal times. RNA was prepared from E18.5, P15 and P90 vestibular organs of *Igf1*$^{-/-}$ and *Igf1*$^{+/+}$ mice and the transcriptome analysed in triplicates using Affymetrix® Mouse Gene 1.1 ST Array Plates. These plates are whole-transcript arrays that include probes to measure both messenger (mRNA) and long intergenic non-coding RNA transcripts (lincRNA), with a coverage of over 28 thousand coding transcripts and over 7 thousands non-coding transcripts. Given the complexity of the data we used two different methods VSN-RMA and mmBGX to analyse and compare the data. This is to better evaluate the number of false positives and to quantify uncertainty of low signals. We identified a number of differentially expressed genes that we described using functional analysis and validated using RT-qPCR. The morphology of the vestibular organ did not show differences between genotypes and no evident alterations were observed in the vestibular sensory areas of the null mice. However, well-defined cellular alterations were found in the vestibular neurons with respect their number and size. Although these mice did not show a dramatic vestibular phenotype, we conducted a functional analysis on differentially expressed genes between genotypes and across time. This was with the aim to identify new pathways that are involved in the development of the vestibular organ as well as pathways that maybe affected by the lack of IGF-1 and be associated to the morphological changes of the vestibular neurons that we observed in the *Igf1*$^{-/-}$ mice.

This article is part of a Special Issue entitled <IEB Kyoto>.

1. Introduction

The adult mammalian inner ear is formed by the auditory and vestibular organs that together form the membranous labyrinth. The vestibular system is responsible of balance and it has two types of sensory organs the cristae and the maculae. The three cristae are

* Corresponding author. Department of Biomedical Science, University of Sheffield, Western Bank, Sheffield, S10 2TN, UK.
E-mail address: m.milo@sheffield.ac.uk (M. Milo).
[1] Co-senior authorship.

http://dx.doi.org/10.1016/j.heares.2015.08.016

Nomenclature

ABR	Auditory brainstem responses
AKT	Protein kinase B
ANOVA	Analysis of variance
APT	Affymetrix Power Tools
Asc	Anterior semicircular canal
CE	Coefficient of error
Cd	Caudal
Co	Cochlea
Ct	Cycle threshold
C-RAF	Raf-1 proto-oncogene, serine/threonine kinase
dB-SPL	Decibel - Sound pressure level
DE	Differential Expression
Do	Dorsal
E (nº)	Embryonic day (nº)
EDTA	Ethylenediaminetetraacetic acid
ERK	Extracellular-signal-regulated kinases
IGF-1	Insulin like growth factor 1
IGF1R	Insulin-like growth factor 1 receptor
IRS1	Insulin receptor substrate 1
KDa	Kilodalton
kHz	Kilohertz
lincRNA	Long intergenic non-coding RNA
Lsc	Lateral semicircular canal
MAPK	Mitogen-activated protein kinase
miR	microRNA
mmBGX	Multi-Mapping Bayesian Gene eXpression
mRNA	Messenger RNA
N	Number of neurons
NF	Neurofilament
Ow	Oval window
P (nº)	Postnatal day (nº)
PANTHER	Protein Analysis Through Evolutionary Relationships
Psc	Posterior semicircular canal
RMA	Robust Multi-array Average
RNA	Ribonucleic acid
Ro	Rostral
RQ	Relative quantification
RT-qPCR	Quantitative reverse transcription polymerase chain reaction
Rw	Round window
SD	Standard deviation
SE	Standard error
SEM	Standard error of the mean
V	Ganglion volume
Ve	Vestibule
vN	Neuronal volume
VsEPs	Short latency vestibular evoked potentials
VSN	Variance Stabilization Normalization
μm	Micrometre

located at the base of semicircular canals and detect angular acceleration, whereas the two maculae detect linear acceleration and gravity. In contrast with the auditory sensory organs, the vestibular sensory patches are highly preserved among species (Fritzsch et al., 2013; Magarinos et al., 2014). Vestibular sensory organs are formed by specialised hair and support cells. The hair cells are the sensory mechanoreceptors and possess a set of sterocilia in their apical surface that allow mechanotransduction. The bipolar neurons of the vestibular ganglia connect the hair cells with the nervous central system through the vestibular nerve (Maklad and Fritzsch, 2003).

In vertebrates, the cochlea and the vestibule develop from a singular patch of ectoderm, the otic placode, which invaginates to form de otic cup that closes to form the otic vesicle or otocyst. This is a transitory embryonic structure that will generate most of the cells of the membranous labyrinth (Bissonnette and Fekete, 1996; Sanchez-Calderon et al., 2007; Magarinos et al., 2014). The neurons for the acoustic-vestibular ganglia delaminate from the otocyst, and they will later differentiate into the acoustic and vestibular ganglia. The projections of vestibular neurons extend to the brainstem nuclei connecting the gravistatic and angular acceleration sensory organs with the brain (Maklad and Fritzsch, 2003). Vestibular disorders greatly affect the quality of life and they increase with ageing. There are several pharmacological interventions under study for the treatment of vestibular disorders, but none of them has been shown to be fully effective (Soto et al., 2013).

Insulin-like growth factor 1 (IGF-1) is an endocrine liver-secreted factor carried by the binding proteins to the body tissues where it binds its high affinity receptor (IGF1R) (Varela-Nieto et al., 2013). IGF-1 deficiency in the mouse causes cochlear cellular alterations (Camarero et al., 2001, 2002) leading to sensorineural hearing loss and a delayed response to acoustic stimuli (Cediel et al., 2006; Riquelme et al., 2010). At the molecular level, IGF-1 deficiency decreases survival signaling whilst increases inflammation and delays differentiation (Sanchez-Calderon et al., 2010). During chicken inner ear development, IGF-1 promotes cell survival and neurogenesis of the acoustic-vestibular ganglion by using mechanisms involving IGF1R, C-RAF and AKT kinases (Aburto et al., 2012; Magarinos et al., 2012). Similarly, IGF-1 has been reported to be anti-apoptotic during human inner ear development (Tafra et al., 2014). IGF system and IGF-1 downstream signaling are also associated with cochlear alterations and hearing loss in mice (Okano et al., 2011; Murillo-Cuesta et al., 2012; Okano and Kelley, 2013). IGF-1 also protects vestibular sensory cells from ototoxic injury and together with other growth factors promotes cell renewal (Kopke et al., 2001; Angunsri et al., 2011). Finally, IGF-1 deficiency is a cause of human deafness (Murillo-Cuesta et al., 2011; Varela-Nieto et al., 2013) and furthermore it has been shown to ameliorate human sudden hearing loss (Nakagawa et al., 2012; Yamamoto et al., 2014).

Despite the increasing knowledge available on the role of IGF-1 in the hearing receptor very little is known of its role in the vestibular system, neither there are many studies exploring the genes involved in the postnatal maturation of the mouse vestibular organ (Abe et al., 2003; Hertzano et al., 2011; Huang et al., 2011). Here we studied gene expression along vestibular development and maturation in wild type and *Igf1*$^{-/-}$ mice. To investigate possible changes at transcription level, we conducted a comparative gene expression study of the vestibular organ of wild type and *Igf1*$^{-/-}$ mice at embryonic day E18.5, and postnatal stages P15 and P90. This analysis shows that the lack of IGF-1 in the vestibule alters the expression of genes that are distinct from those differentially expressed in the cochlea (Sanchez-Calderon et al., 2010). Furthermore the expression patterns of several microRNAs (miRs) are shown to be associated to vestibular maturation and some of them are altered in the *Igf1*$^{-/-}$ mouse.

2. Materials and methods

2.1. Mouse handling and genotyping

Mice heterozygous for *Igf1* gene were maintained on a hybrid MF1 and 129/sv genetic background to increase *Igf1*$^{-/-}$ mutant survival (Liu et al., 1993). Mouse genotypes were identified using the REDExtract-N-AmpTMTissue PCR Kit (Sigma–Aldrich, St. Louis, MO) according to the manufacturer's instructions. PCR was performed as follows: 1 cycle of 94 °C for 10 min; 30 cycles of 94 °C for 1 min, 59 °C for 1 min, 72 °C for 1 min; and a final elongation step at 72 °C for 10 min. For *Igf1* genotyping, *Igf1* forward -5′ GTCTAACACCAGCCCATTCTGATT 3′- and *Igf1* reverse -5′ GACTCGATTTCACCCACTC 3′-; neomycin forward -5′ GCTTGGGTGGAGAG GCTATCC 3′- and neomycin reverse -5′ CCAGCTCTTCAGCAATATCACGGG 3′ primers were used simultaneously with no evidence of interference and produced a 250-bp and 658-bp amplicons respectively. The animals were fed a standard diet, drinking water ad libitum and housed in accordance with the recommendations of Federation of European Laboratory Animal Science Associations. All animal experimentation was conducted in accord with Spanish and European legislation (EU directive 2010/63/EU) and approved by the Animal Care and Use Committees of Spanish National Research Council (CSIC).

2.2. Evaluation of vestibular and auditory functions

Inner ear functions were studied in adult young (P30 to P150) wild type and null mice. Vestibular function was evaluated with a primary pipeline comprising a battery of tests for a broad characterization of the vestibular phenotype, adapted from standard protocols (Hardisty-Hughes et al., 2010) (http://empress.har.mrc.ac.uk/), as described previously (Munoz-Espin et al., 2013). The primary vestibular phenotyping test panel detects gross abnormalities. Specialised vestibular tests that provide detailed functional information on hair cell function (Knox et al., 1993; Freeman et al., 2000) are not included in the basic screen. Minor defects are not detected with this type of panel but cannot be excluded. First, mice were observed for abnormal behavioral signs indicative of vestibular disorders, including circling, head bobbing, abnormal gait, etc. Then, we tested the ability of mice to reach a presented horizontal surface and the presence of abdominal forward curling. Next, we carried out the contact righting and the air righting tests to evaluate the ability of mice to reorientate the body from an inverted position. Finally, a swimming test was carried out to find out abnormal swim behavior including vertical, circular or side swim, or immobile floating. The following scores were used for the vestibular tests: i) General observation: 0, normal behavior; 1, behavioral signs indicative of a vestibular disorder. ii) Trunk curl test: 0, normal reaching response, forelimbs reach toward the approaching surface; 1, absent reaching response; 2, slight spinning on their axis, trunk curling, and limb grasping; 3, trunk circling. iii) Contact righting test: 0, mouse ignores the inverted surface and rotates back to its upright position; 1, mouse remains inverted. iv) Air righting test: 0, mouse rotates back to its upright position during falling; 1, mouse falls inverted. v) Swimming test: 0, normal swimming (mouse body elongated, the tail propels in a flagella-like motion); 1, irregular swimming (vertical, in a circle, on side, unbalanced); 2, immobile floating; 3, underwater tumbling.

In parallel, auditory brainstem responses (ABR) were obtained under anesthesia with Ketamine® (Imalgene, Merial, France) 75 mg/kg and Xylazine (Rompum® 2%, Bayer, Germany) 5 mg/kg in a sound-attenuating chamber, with a TDT System 3 workstation (Tucker Davis Technologies, Alachua FL, USA), as described previously (Cediel et al., 2006). Tone-burst (8, 16, 28, and 40 kHz) and click stimuli (1–16 kHz) were presented at decreasing intensities in steps from 90 dB SPL to 10 dB SPL with a MF-1 magnetoelectrostatic speaker placed 5 cm from the animal's ear. Electroencephalographic responses were recorded using needle electrodes (Spes Medica, Milan, Italy) placed in the vertex (+), mastoid area (−) and the back (ground), and then amplified by a factor of 1 × 106. Auditory thresholds, latencies of peaks I–V, and interpeak latencies were analysed.

2.3. Vestibular organ dissection, inner ear clearing, histology and immunohistochemistry

Mice were euthanised with pentobarbiturate injection (Dolethal®, Vetoquinol S.A., France) and the skin of the head was snipped from back to front and pulled towards the nose. The skull was cut from the occipital bone along the sagittal suture and the brain was removed to reveal the bony labyrinth. The inner ear was separated by gross dissection and then transferred to a culture dish to continue the dissection under the stereomicroscope (Leica MZ75, Leica Microsystems, Wetzlar, Germany) were the bulla was removed. Next, the vestibular and cochlear components of the inner ear were separated by a surgical section along the imaginary line connecting the distal ends of the oval and round windows. By following this procedure the macular and crests components were included. All the samples were identically manipulated and treated, independently of the age.

Inner ears of P30 *Igf1*$^{+/+}$ and *Igf1*$^{-/-}$ mice were dissected out and fixed for 2 h in Bodian's fixative for inner ear clearing. After washing in distilled water for 30 min, they were placed in 70% ethanol for 24 h with rotation, and changed to 3% KOH refreshing daily until soft tissues were dissolved. The samples were cleared for the study of the bony labyrinth in a solution of glycerol, 70% ethanol and benzyl alcohol (ratio 2:2:1) for 24 h with rotation and stored in glycerol and 70% ethanol (1:1) until photographed (Kuhn et al., 2012). The vestibular tissue was dissected and cleaned from mesenchymal tissue as discussed above, however variable traces of contamination in some samples can never be excluded. It is improbable that these variable minimal amounts of mesenchyme have a strong bias in our data analysis. Even though to ensure that our dataset did not contain confounding signals, we conducted Gene Set Enrichment Analysis (GSEA) (http://www.broadinstitute.org/gsea/index.jsp), (Subramanian A, Tamayo et al., 2005; Mootha et al., 2003) on the data for enrichment of mesenchymal-specific markers.

For histological studies adult mice were deeply anesthetised and transcardially perfused with 4% paraformaldehyde in 0.1 M phosphate-buffered saline (PBS, pH 7.4). The inner ear was dissected out, post-fixed in fresh fixative solution for 12 h and decalcified for 2 weeks with 10% EDTA. For each mouse, one inner ear was embedded in paraffin following standard procedures. Paraffin sections (5 μm) of vestibular organs from *Igf1*$^{+/+}$ and *Igf1*$^{-/-}$ mice were processed for haematoxylin/eosin or Nissl-staining using cresyl violet to study general cytoarchitecture, as described (Camarero et al., 2001, 2002).

2.4. Stereology

Mice were anesthetised with CO_2 on dry ice (P5) or by intraperitoneal injection of 0.12 mg/g ketamine hydrochloride (P20), and perfused transcardially with 4% paraformaldehyde in 0.1 M phosphate buffer (PB). The procedure resembled that used in an earlier study of the spiral ganglion (Camarero et al., 2001). Heads were removed, post-fixed for 3 days in the same fixative, decalcified in 0.3 M EDTA pH 6.3, for 3 days (P5) or 7 days (P20),

dehydrated, defatted, sagitally divided into two halves, and embedded in low viscosity nitrocellulose (Celloidin; Fluka, Buchs, Switzerland). Celloidin blocks containing the hemicrania were serially cut at 50 μm using a sliding microtome, following different planes of section for each side: left hemicranias were sectioned along the sagittal plane and right hemicranias along the horizontal plane. Sections were collected and stored in 70% ethanol, and every second section was mounted and Nissl-stained using 1% cresyl violet. The total volume of the vestibular ganglion, the total neuron number, and the mean soma volume and size distribution of ganglion neurons were estimated on 20 mice (3–5 mice of each age and genotype, except just one case of P5 *Igf1*$^{+/-}$ animals). The ganglion volume (V) was obtained by point counting and the Cavalieri estimator (Gundersen et al., 1988), considering "ganglionar area" groups of neurons with more than two juxtaposed neuron bodies; the absolute number of neurons (N) was estimated by the optical fractionator (West, 1993) using nucleoli as counting units, and the mean neuronal volume (vN) and distribution of individual volume estimates were estimated by the planar rotator (Tandrup et al., 1997). All measurements were performed using an interactive computer system that included a high precision motorised microscope stage, a 0.5 μm resolution z-axis reader (microcator VZR 401; Heidenhain, Traunreut, Germany), an Olympus DP70 video camera, and a high-resolution video monitor. For cell counting and cell body volume estimation, a planapochromatic 100× oil immersion lens with a 1.4 numerical aperture (S-Plan Apo 100; Olympus Optical, Hamburg, Germany) was used. The interactive test grids and control of the motorised stage were provided by the CAST stereological software package (Visiopharm, Hørsholm, Denmark). The investigator who performed all the measurements was blind to the group. A second investigator independently repeated some measurements, which yielded an interobserver variability below 4% (for V estimations) and 7% (for N estimations). The precision of the estimations of N and V was assessed by estimating the coefficient of error (CE) as described for systematic random samples (Cruz-Orive, 1999). The average CEs obtained were always below 11% and 4% for N and V estimations, respectively. The precision of the estimates of vN was evaluated by calculating the CE (which always remained below 8%) using ordinary statistics for independent observations. Cell and ganglion volume estimates were not corrected for shrinkage.

All plots represent mean ± SD. Since less than 2% mean differences between sides were found in each group, V and N values represent right-left averages for each animal. After testing for normality and homogeneity of variances, comparisons between groups were made with two-tailed Student's t test, or with Kruskal–Wallis ANOVA by ranks. The cumulative frequency distributions of vN values were compared with the Kolmogorov–Smirnov test.

2.5. RNA isolation and array experiment

Igf1$^{+/+}$ and *Igf1*$^{-/-}$ mice were studied at different time points (E18.5, P15 and P90) to follow their progression from embryonic stage to adult mice. RNA extraction from mice vestibular organs was performed with the Trizol® (Life Technologies, Carlsbad, CA) method, subsequent treatment with DNase (DNA-free, Ambion, Carlsbad, CA) and purification columns (RNeasy mini kit, Qiagen, Valencia, CA). RNA quality was determined by Agilent 2100 Bioanalyzer. Each sample was prepared from the pool of two mice and the transcriptome analysed in triplicates using Affymetrix® Mouse Gene 1.0 ST Array Plates (Affymetrix, Santa Clara, CA). These plates are whole-transcript arrays that include probes to measure both messenger (mRNA) and long intergenic non-coding RNA transcripts (lincRNA), with a coverage of over 28 thousand coding transcripts and over 7 thousands non-coding transcripts. The raw and the processed data are available from the Gene Expression Omnibus database (http://www.ncbi.nlm.nih.gov/geo/). GEO accession number: GSE65202.

Table 1
ABR thresholds (mean ± SD, in dB SPL) in response to click and tone burst (from 8 to 40 kHz) stimuli from 4 to 5 months-old *Igf1*$^{-/-}$, *Igf1*$^{+/-}$ *and Igf1*$^{+/+}$ mice.

	Click	8	16	20	28	40
Igf1$^{+/+}$	20 ± 5	28 ± 4	24 ± 2	27 ± 5	30 ± 4	36 ± 7
Igf1$^{+/-}$	20 ± 5	26 ± 2	24 ± 4	27 ± 7	31 ± 6	37 ± 10
Igf1$^{-/-}$	62 ± 12	66 ± 11	49 ± 13	48 ± 10	59 ± 10	68 ± 11

2.6. Microarray data analysis

An initial analysis of data was performed with different packages available as part of Bioconductor (http://www.bioconductor.org/) and included data pre-processing with Affymetrix Power Tools (APT), which used the standard version of Robust Multi-array Average (RMA) (Irizarry et al., 2003). This approach did not detect significant changes of gene expression due to the high *signal to noise* ratio present in the data. Subsequently the data was analysed and then compared using two different methods: a variance stabilizing normalization RMA (VSN-RMA) (Huber et al., 2002) and Multi-Mapping Bayesian Gene eXpression (mmBGX) (Turro et al., 2010). Both methods use different approaches from the APT software: VSN-RMA adds to RMA quantification a calibration step, to reduce the background noise and the variance in the data; mmBGX is a probabilistic method that is able to quantify more accurately false positives and uncertainty of gene expression estimates. VSN-RMA consists in two-steps analysis: i) a variance stabilization method for calibrating experimental factors and normalization; ii) a summary of the gene expression using RMA. However, VSN-RMA only addresses the dependence of the variance on the mean gene expression intensity and that might be not sensitive enough to detect small changes and to handle non-linear noise. Since the vestibular organ is very complex and there are several gene specific properties and/or changes of the tightness of transcriptional control in the organ, the variance in the data can be affected by different factors and the accuracy of the gene expression estimates might be highly compromised. Therefore to improve the accuracy of the estimates and quantify their uncertainty to reduce the number of false positives in the Differential Expression (DE) analysis, we repeated the analysis of the data using a full hierarchical Bayesian approach as implemented in mmBGX. Gene expression estimates calculated by mmBGX are summaries of transcript expression, which are mapped onto same genes. Those summaries are estimated probability values of gene expression, calculated using a probabilistic model of the transcripts measures. They also have a measure of associated uncertainty, which reflects the error in that estimates. Biological replicates were combined within mmBGX using its Hierarchical Bayesian model. The combined expressions as estimated by mmBGX, were used to perform DE analysis and to rank the differentially expressed genes, using the estimated uncertainty of each gene expression estimates. In the DE analysis we chose targets with a fold change greater than 0.9 and smaller than −0.9. From this initial filter we also selected the targets with the lowest ranking as indicated by the mmBGX method (Turro et al., 2010).

Given the complexity of the vestibular organ, we wanted to

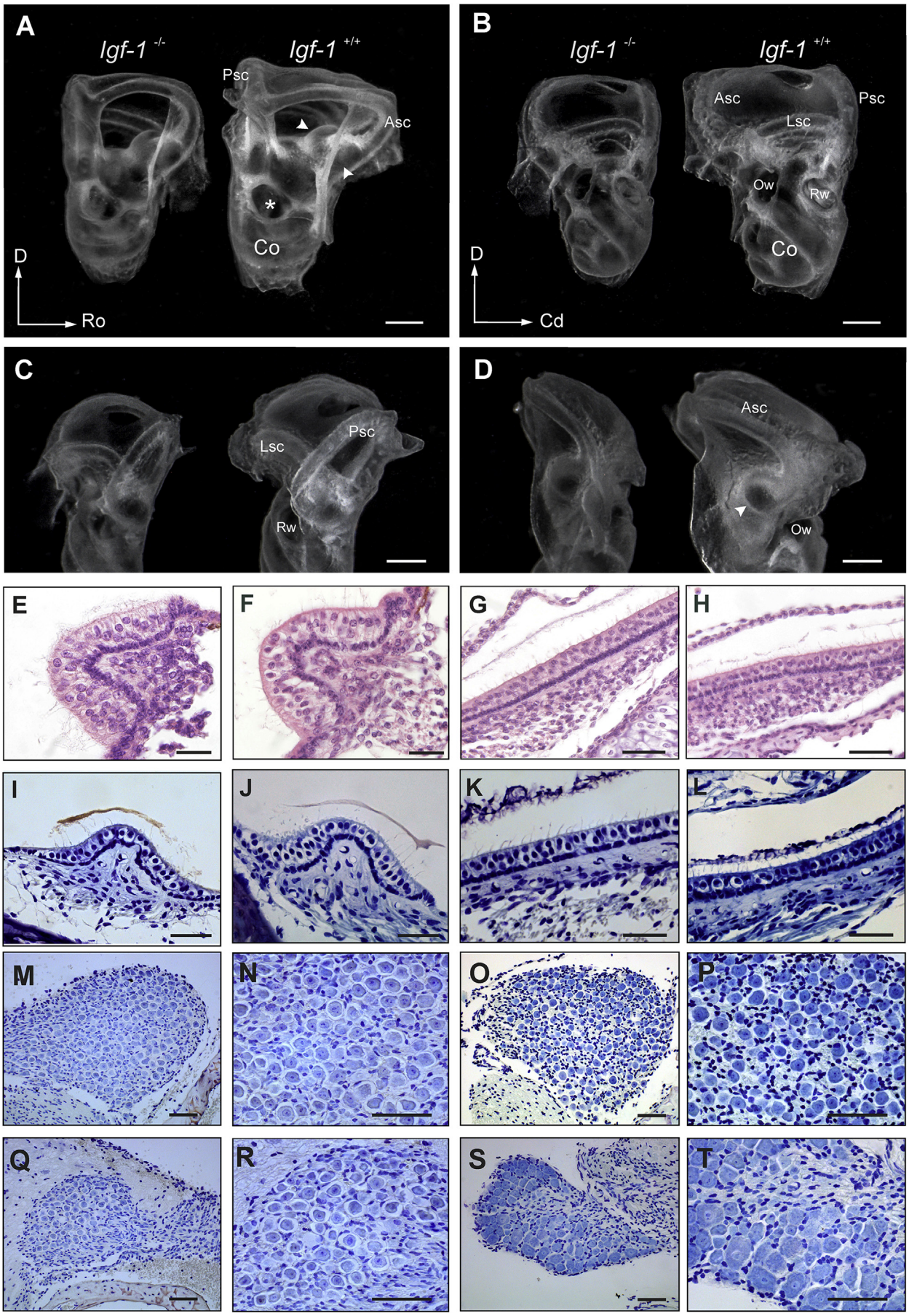
A
Igf-1 -/-
Igf-1 +/+
Psc
Asc
Co
D
Ro
B
Igf-1 -/-
Igf-1 +/+
Asc
Psc
Lsc
Ow
Rw
Co
D
Cd
C
Lsc
Psc
Rw
D
Asc
Ow
E
F
G
H
I
J
K
L
M
N
O
P
Q
R
S
T

quantify the weight of confounding factors, like potential mesenchymal contamination and bone-related signals. Although at the pre-natal and post-natal stages studied, the vestibular bony and membranous labyrinths are already formed, there are cell types, including osseous cells, still on-going differentiation processes. With this in mind, we conducted Gene Set Enrichment analysis (GSEA) on the whole dataset prior selection and post normalisation process. This is to ensure that: i) there is no biased signal due to different amounts of mesenchymal tissue contributing to the sample after our dissection procedure; and ii) to estimate the contribution of osseous tissue to the data.

To implement the GSEA we used two sets of gene markers, one for mesenchymal specific markers and one for bone-related specific markers. These genes are listed in Tables S1 and S2 from supplemental material, respectively. The parameters we used to set the Enrichment analysis were as follow: weighted scoring scheme, fold changes as metric and 1000 random permutations. The data used was the full processed and normalised dataset. Results from GSEA showed that there was no enrichment of mesenchymal markers when wild type are compared to null mice at the ages studied (Figures S1–S3, supplemental material). Thus we can be confident that signals from variable traces of such tissue have been normalised across the dataset. Parallel GSEA analysis conducted for bone specific markers, showed that there was no enrichment of bone markers at E18.5 and P90 but there was enrichment of about 50% of the specific bone markers chosen at P15 (Figs. S1–S3, supplemental material). This possibly reflects the postnatal development of the vestibular bony labyrinth, as discussed above. Detailed data of the GSEA conducted on the data is summarised in Table S3.

The final list of Differentially Expressed targets comprised the ones that passed the above filtering steps and among those, we gave priorities to the ones that were identified by more than one method. The lists of targets were clustered using Hierarchical Clustering with Euclidean distance as similarity measure. Heatmaps of the correlations were built using z-score of the expression values. The Z scores represent the dispersion around the overall mean of the data and weighted by its standard errors.

Functional analysis of differentially expressed genes was performed using the PANTHER (Protein Analysis Through Evolutionary Relationships) classification system (Mi and Thomas, 2009).

2.7. Validation by RT-qPCR

RNA samples from mice vestibules used for the array study were further used for its validation. RT-qPCR was conducted on Applied Biosystems 7900 HT and TaqMan Gene Expression and MicroRNA Assays (Life Technologies, Carlsbad, CA) were used for amplification of differentially expressed genes and miRs selected from the study of the array according to the expression in the vestibule across different time points and to reported relation with deafness, inner ear expression or IGF system. The following miRs and genes were studied by RT-qPCR: *miR-18*, *miR-148a*, *miR-181a-1*, *Ttr*, *Ucp1*, *Mitf*, *Cidea*, *Enpp2*, *Pde1c*, *Dnajc5b* and *Grxcr1*. The ribosomal phosphoprotein P0 (*Rplp0*) was used as endogenous control gene to normalize results. Relative quantification (RQ) between *Igf1*$^{-/-}$ and *Igf1*$^{+/+}$ mice was determined by the $2^{-\Delta\Delta Ct}$ method, where $\Delta\Delta Ct = \Delta Ct_{\text{target assay}} - \Delta Ct_{\text{reference assay}}$. Data were expressed as RQ mean ± standard error (SE), and the results were considered significant at $p < 0.05$. Statistical significance was estimated by Student's t test after using the F test to confirm equality of variances.

3. Results

3.1. Functional and morphological characterization of the auditory and vestibular systems of the *Igf1*$^{-/-}$ mouse

Igf1$^{-/-}$ mice have been reported to fail in the late differentiation processes undergone postnatally by spiral neurons, leading to progressive neuronal loss and causing sensorineural deafness (Cediel et al., 2006; Rodriguez-De La Rosa et al., 2012; Fuentes-Santamaria et al., 2014). As expected, adult null mice at the ages studied here from P30 to P150 presented higher ABR thresholds in response to click and tone burst stimuli than *Igf1*$^{+/+}$ wild type mice (data not shown and Table 1).

In contrast, vestibular tests performed in parallel at the same ages in *Igf1*$^{-/-}$, *Igf1*$^{+/-}$ and *Igf1*$^{+/+}$ mice (n = 5/genotype) revealed a normal vestibular phenotype without differences among them (data not shown). Our data indicate that no major vestibular functional alterations were present during this time window, whilst auditory function defects persisted. The inner ear of adult *Igf1*$^{-/-}$ mice showed altered general morphology and smaller size than those of *Igf1*$^{+/-}$ and *Igf1*$^{+/+}$ mice, but not major cytoarchitecture aberrations (Riquelme et al., 2010). Accordingly, the gross vestibular morphology of both genotypes was similar and they did not show striking cellular differences being all the vestibular cellular types present and connected (data not shown). The data on the anatomy of the *Igf1*$^{-/-}$ and *Igf1*$^{+/+}$ ears is summarised in Fig. 1. The cytoarchitecture of the vestibular organ was also similar in *Igf1*$^{-/-}$ and *Igf1*$^{+/+}$ mice (Fig. 1). A stereological analysis of the vestibular ganglion showed apparent increases in ganglion volume and neuron number with age in both genotypes (Fig. 2). However, while the ganglion did not differ in size between genotypes at any given age, the age-dependent increase in neuron number at P20 was significantly smaller in null mice (13%) compared to wild type animals (34%) (Fig. 3). Even more notable differences between genotypes were observed in the distribution of neuronal soma sizes (Fig. 3). Whilst this distribution was monomodal and similar in shape in all groups, there were highly significant differences between age and gene groups, with median cell volume values 30% and 33% smaller in null mice compared to wild type mice at P5 and P20, respectively. To summarise, the results shown here suggest that the neural alterations observed are largely compensated at the functional level at the ages that we considered in this study.

Fig. 1. Comparative anatomy of the *Igf1*$^{-/-}$ *and Igf1*$^{+/+}$ inner ears. A–D) Cleared inner ears of *Igf1*$^{-/-}$ *and Igf1*$^{+/+}$ mice (medial view, A; lateral view, B; caudal view, C; rostral view D). *Igf1*$^{-/-}$ inner ears showed a normal aspect but differences in size (small in null mouse) and in the 3D conformation, with shorter semicircular canals than the wild types. Abbreviations are: Co, cochlea; Asc, Lsc and Psc, anterior, lateral and posterior semicircular canals; Do, dorsal; Ro, rostral; Cd, caudal; Ow, oval window; Rw, round window. Arrowhead, osseous ampullae; asterisk, orifice of the internal acoustic meatus, origin of VIIIth cranial nerve. E-H) Anatomy of the vestibular cristae and maculae of null (E, G) and control (F, H) mice at P5, haematoxylin/eosin staining of paraffin sections. There are no apparent differences in the morphology of cristae and maculae among both genotypes that present normal hair cells and supporting cells. I-T) Anatomy of the vestibular cristae, maculae and ganglion at adult age of null (I, K, M, N, Q, R) and wild type (J, L, O, P, S, T) mice, cresyl violet staining of paraffin sections, showing the cytoarchitecture of the vestibular neurosensorial component of the inner ear. There are no apparent differences in the morphology of cristae and maculae among both genotypes that present normal hair cells and supporting cells. The vestibular ganglion shows a heterogeneous size of neurons (T). Scale bars: A–D, 0.5 mm; E–H, 25 μm; I–T, 50 μm.

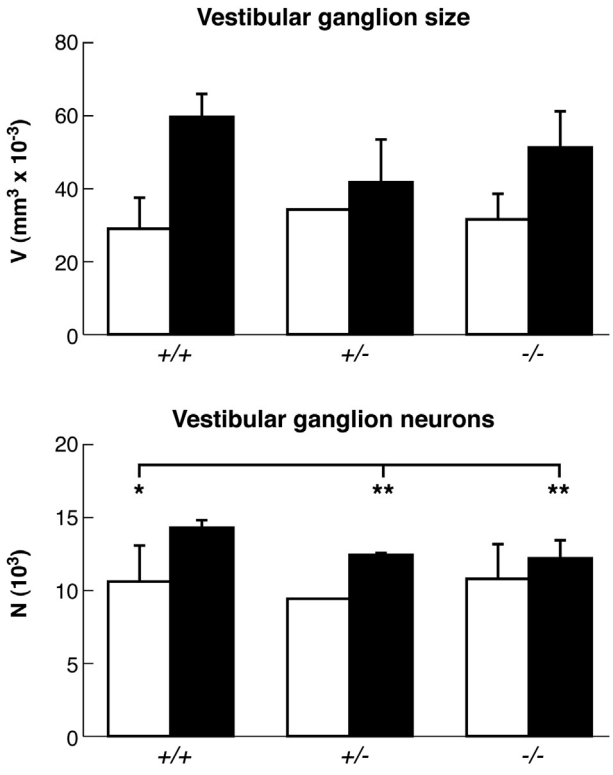

Fig. 2. Vestibular ganglion size and sensory neurons in *Igf1*$^{-/-}$, *Igf1*$^{+/-}$ *and Igf1*$^{+/+}$ mice. Volume of the vestibular ganglion (top) and total number of primary sensory neurons (bottom) in P5 (empty bars) and P20 (shaded bars) mice of different genetic backgrounds (mean ± SD). The ganglion grew in size with age in all groups, with no differences between genotypes. Neuron numbers also showed apparent increases with age in all groups, but this change reached significance only for wild type mice (t-test, 34%, p = 0.013), whose neuron numbers were very significantly higher than in *Igf1*$^{-/-}$ (17%, p = 0.007) and *Igf1*$^{+/-}$ (15%, p = 0.003) mice.

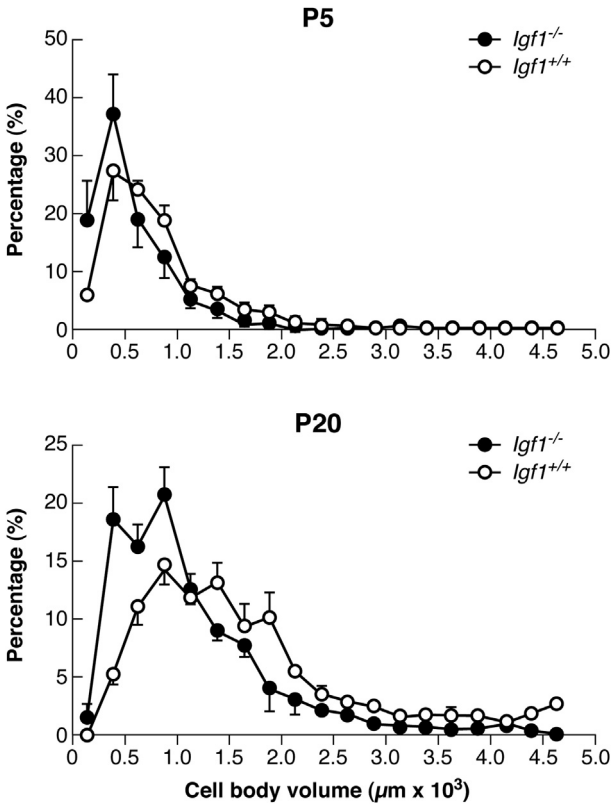

Fig. 3. Differences in cell body volume distribution of vestibular ganglion neurons in *Igf1*$^{-/-}$ *and Igf1*$^{+/+}$ mice at ages P5 and P20. Error bars represent SEM among animals for each volume class. While neurons grew in size with age in all groups, a Kruskal–Wallis test showed highly significant differences between age and gene groups (χ^2 = 53.91, p = 0.000), with null mice displaying significantly smaller neuron populations than wild type mice at both P5 (p = 0.008) and P20 (p = 0.023). The Kolmogorov–Smirnov test applied to the cumulative distributions of all cell volumes pooled confirmed highly significant differences between groups (p = 0.000).

3.2. Comparative gene expression analysis in the *Igf1*$^{-/-}$ mouse

We then analysed the transcriptomes of wild type vestibular organs and *Igf1*$^{-/-}$ mice, to identify differences in gene expression in the vestibular organ of *Igf1*$^{-/-}$ compared to wild type mice at different ages. IGF-1 is essential for the postnatal maturation and differentiation of the cochlea (Camarero et al., 2001, 2002; Sanchez-Calderon et al., 2010). Consequently, the vestibular system was studied in a late prenatal stage (E18.5), an intermediate stage of ongoing postnatal maturation (P15) and in a young adult age (P90). There were striking differences in the *Igf1*$^{-/-}$ mouse vestibular gene expression profile among the embryonic and postnatal ages. The vestibule of *Igf1*$^{-/-}$ mouse showed a distinct gene expression signature, which included a set of miRs that were differently expressed in the null mice (Table 2).

Comparative gene expression analysis between wild type and *Igf1*$^{-/-}$ mice identified differences in the pattern of gene expression across all time points selected for this study. A total of 211 differentially expressed transcripts were identified in total, of which 129 mapped onto annotated genes. A number of 69 genes where identified as differentially regulated in the vestibule of *Igf1*$^{-/-}$ mouse at embryonic stage E18.5, whilst 39 and 21 were differentially regulated at postnatal stages P15 and P90, respectively (Table 2). In Tables 3 and 4 we show those differentially expressed genes whose expression and/or function have been associated with the inner ear.

We found 5 targets that stayed differentially expressed between wild type and *Igf1*$^{-/-}$ mice at E18.5 and P15: *Ampd1, Myl2, Mybpc2, Col6a5* and *Ucp1*. There were 6 targets that stayed differentially expressed at E18.5 and P90: *mir18, Rsp24, Atpaf1, Npm1, Tmsb15l* and *Ucp1*. At P15 and P90 that were only 2 genes that stayed differentially expressed: *Ttr* and *Ucp1*. It is worth noting that *Ucp1* stayed differentially expressed across all the time points (Fig. 4, panel A).

We clustered the data from the mmBGX analysis, using hierarchical clustering with similarity measure set as Euclidean distance and using the full set of transcripts expressions prior filtering. We looked at the clustering of the whole transcriptome for the two genotypes and for the time of development (Fig. 4, panel B). This analysis revealed that the gene expression signatures held in the transcriptome were able to separate the embryonic from the postnatal stages, but would cluster together the genotypes rather than the stages of development at P15 and P90. This is shown by the dendrogram in Fig. 4, panel B, where the vertical distances on each branch of the dendrogram represent grade of the similarity between the samples.

The heatmap of the hierarchical clustering of the differentially expressed genes for a selected time point also showed same association as per whole transcriptome. Fig. 5 shows the clustering of the differentially expressed genes at E18.5 and the correspondent expression values in the other two time points. Fig. 5, clearly shows the wide changes of expressions of selected targets that are deregulated at embryonic stage E18.5 and equalised in later stages. Fig. 6 and Fig. 7 shows similar scenarios for the list of selected genes at P15 and P90, respectively.

Table 2
Summary of differentially expressed (DE) analysis across *Igf1*$^{-/-}$ *and Igf1*$^{+/+}$ genotypes at different time points. The symbol ↑ indicates up-regulation, whilst the symbol ↓ indicates down-regulation.

	DE transcripts	Annotated transcripts	DE miRs	↑ genes in *Igf1*$^{-/-}$	miR in *Igf1*$^{-/-}$
E18	104	69	*miR-148a*	47	↓ *miR-148a*
			miR-18		↓ *miR-18*
			miR-181a-1		↓ *miR-181a-1*
			miR-346		↑*miR-346*
P15	64	39	*miR-144*	51	↓ *miR-144*
P90	43	21	*miR-125b-1*	17	↑ *miR-125b-1*
			miR-18		↑ *miR-18*
			miR-361		↑ *miR-361*
			miR-411		↑ *miR-411*

Table 3
Genes selected for RT-qPCR validation. Genes were selected according to their expression in the vestibule array across different time points and to reported relation with deafness, inner ear expression or IGF system in the bibliography. FC, fold change.

Gene symbol	Gene	FC E18.5	FC P15	FC P90	Function
miR-148a	microRNA 148a	−1.45	–	–	*miR-148a/152* inhibit cell proliferation and tumor angiogenesis through targeting IGF-1R and IRS1 and inhibiting AKT and ERK signaling pathways in breast cancer cell lines (Xu et al., 2013).
miR-181a-1	microRNA181a-1	−1.16	–	–	*miR-181a* is highly expressed in cochlear and vestibular epithelium of P0 C57Bl/6J mice (Rudnicki et al., 2014) and it seems to play a key role in hair cell regeneration in explants of chicken auditory epithelia (Frucht et al., 2011).
Mitf	Microphthalmia-associated transcription factor	−1.01	–	–	*Mitf* mutations are associated with the human rare diseases Waardenburg syndrome type 2A (WS2A) (ORPHA895) and Tietz syndrome (ORPHA42665). WS2A is characterized by sensorineural hearing loss, abnormal pigmentation of the hair and skin (Liu et al., 1995) that are caused by the lack of melanocytes in skin and inner ear (Shibahara et al., 2001). Tietz syndrome is characterized by congenital profound bilateral sensorineural hearing loss and generalized albino-like hypopigmentation of skin, eyes and hair (Smith et al., 2000).
Cidea	Cell death-inducing DNA fragmentation factor, α subunit-like effector A	1.00	–	–	*Cidea* acts as a C/EBPβ co-activator in mammary epithelial HC11 cells to modulate C/EBPβ downstream target genes including *Igf1* (Wang et al., 2012) and acute phase cytokines (Ruffell et al., 2009).
miR-18	microRNA 18	−0.94	–	0.90	*miR-18a* is expressed in the cochlear spiral ganglion neurons, in hair cells and supporting cells of the vestibular sensory epithelium in new born mice. *miR-18a* plays a key role in zebrafish inner ear development and morphogenesis (Friedman et al., 2009).
Ucp1	Uncoupling protein 1 (mitochondrial, proton carrier)	1.38	−1.70	1.16	UCP1, UCP2, UCP3, Slc25a27 (UCP4) and Slc25a14 (UCP5) mRNAs are expressed in the vestibular and spiral ganglion of 4-week-old C57BL/6, CBA/J and BALB/c mice (Kitahara et al., 2005).
Enpp2	Ectonucleotide pyrophosphatase-phosphodiesterase 2	–	−0.99	–	*Igf2*, *Igfbp2* and *Enpp2* are a set of estrogen-responsive genes in the 8-week-old rat hippocampus (Takeo et al., 2009).
Pde1c	Phosphodiesterase 1C	–	0.92	–	IRS1 and PDEC1 are co-expressed in the sensory epithelial hair cells of the human saccule (Degerman et al., 2013).
Dnajc5b	DnaJ (Hsp40) homolog, subfamily C, member 5 β	–	–	0.92	*Dnajc5b* is one of the main differentially expressed genes in inner hair cells of 1-month- old CBA/J mice (Liu et al., 2014).
Grxcr1	Glutaredoxin, cysteine rich 1	–	–	1.11	*GRXCR1* mutations in man are responsible for sensorineural autosomal recessive nonsyndromic hearing impairment that can be accompanied by vestibular dysfunction (Schraders et al., 2010). In early postnatal mice *Grxcr1* is expressed in the sensory epithelia of the inner ear and it mutations in pirouette mice result in hearing loss and vestibular dysfunction due to neuroepithelial defects in the inner ear (Odeh et al., 2010).
Ttr	Transthyretin	–	−2.45	1.05	A transthyretin variant Leu12 Pro is associated with systemic and neuropathic amyloidosis in man (Brett et al., 1999). Human transthyretin amyloidosis (ser44) in man has been linked with headache, hearing loss, and peripheral neuropathy (Klein et al., 1998).

Functional analysis of the selected transcripts was conducted using the PANTHER classification system to discover enriched pathways in the differentially expressed targets. Genes have been classified according to pathways for E18.5 and P15 (Fig. 8, panels A and B) or molecular function for P90 (Fig. 8, panel C). PANTHER classification system is a rich collection of protein families that have been subdivided into subfamilies based on their functional interactions and associated genes. The association of ontology terms and pathways is based on how correlation values between the subfamilies and the specific protein function associated to the genes. PANTHER uses sophisticated statistical tools to model interactions of the protein families collected and to define a ranked list of the association with the ontologies and pathways. These models also allow to define significance of these associations against randomness, based on the size of the list of genes inputted and of the specific characteristics of the reference genome. In Fig. 8 we summarise the functional analysis on the list of differentially expressed genes, using PANTHER classification system. The bar charts in Fig. 8, panel A and B, describe the pathways that are significant over randomness, given the size of the inputted list of targets, for ages E18.5 and P15. The y-axis defines the number of genes from the input list that fall into the specific pathways, which are categorised in the x-axis. At stage P90 the list of differentially expressed genes had no enriched pathways that were statistically significant. This is most probably due to the fact that the list is rather small and statistical significance could not be reached. For this reason, Fig. 8, panel C, summarises the proportion of enriched molecular functional groups associated to genes in the list. The pie

Table 4
Genes differentially expressed in the vestibular system of the *Igf1*$^{-/-}$ mouse at different time points and, whose function or expression in the inner has been reported previously in the bibliography. FC, fold change.

Gene symbol	Gene	FC E18.5	FC P15	FC P90	Function & inner ear expression
Gtf3c2	General transcription factor IIIC, polypeptide 2, beta	−1.29	–	–	*Gtf3c2* is a transcription factor expressed in the inner ear, middle ear and labyrinth of the E14.5 mouse embryo (Visel et al., 2004).
Hmgb1	High mobility group box 1	−0.90	–	–	*Hmgb1* is a late mediator of inflammation and a signal of tissue damage. It is involved in the epithelial remodeling of the organ of Corti after ototoxic insult (Ladrech et al., 2013). *Hmgb1* is expressed in the mouse E13.5 inner ear (Gray et al., 2004).
Tmsb15	Thymosin beta 15	−1.20	–	0.94	*Tmsb15* is an actin-binding protein involved in the regulation of cell migration (Banyard et al., 2009). *Tmsb15l* has a role in chicken myogenesis (Chankiewitz et al., 2014) and it is expressed in the bony labyrinth with a regionally restricted pattern in the E14.5 mouse embryo (Diez-Roux et al., 2011).
Kcne2	Potassium voltage-gated channel	–	−1.01	–	KCNQ1 and KCNE proteins play important roles in the homeostasis of K^+ in a variety of tissues. In the inner ear, KCNQ1 and KCNE1 maintain the high concentration of K^+ in the endolymph. *Kcne2* expression has been reported in the E14.5 mouse inner ear (Visel et al., 2004). The inner ear of rats with mutated *Kcnq1* shows severe morphological abnormalities, which are associated with deafness and imbalance (Gohma et al., 2006).
Pou1f1	POU domain, class 1, transcription factor 1	–	1.38	–	*Pou1f1* is a pituitary-specific transcription factor member of the POU family. It is responsible for pituitary development and hormone expression. The *Pou1f1* deficient mouse presents pituitary thyrotropin deficiency and deafness (Fang et al., 2012).
Upk1b	Uroplakin 1B	–	–	0.92	*Upk1b* belongs to the tetraspanin family of membrane proteins and it is expressed in the E14.5 mouse embryo pharyngo-tympanic tube (Eustachian tube) (Diez-Roux et al., 2011).
Kcnma1	Potassium large conductance calcium-activated channel, subfamily M, alpha member 1	–	–	0.96	The *Kcnma1* gene encodes for the pore-forming alpha subunit of the Ca^{2+}-activated potassium channels (BK channels) and it is expressed in the P21 mouse cochlea (Beisel et al., 2007). Mutant *Bk*$^{-/-}$ mice with targeted disruption of the *Kcnma1* gene present ataxia and neurologic deficits (Sausbier et al., 2004). Targeted deletion of BK channels in hair cells (*Hc-Bk*$^{-/-}$) has shown its role in central auditory processing (Kurt et al., 2012).

chart identifies the relative proportions with respect to the total number of genes in the inputted list. Specific details of functional analysis are collected in Table S4, S5 and S6 in supplementary material, for statically significant enriched pathways at E18.5 and P15 and statistical significant enriched molecular function groups at P90, respectively.

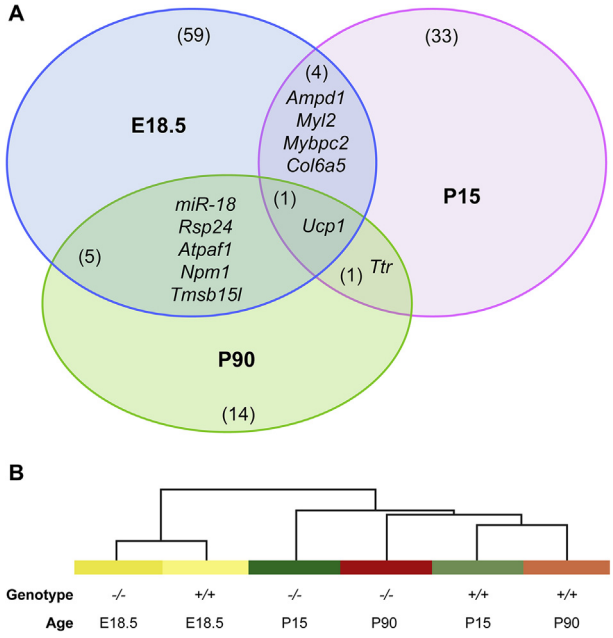

Fig. 4. Summary of transcriptome analysis of the mammalian vestibular organ. A) Summary of differentially expressed transcripts and how they are compared across different stages of development. Numbers in the diagrams represents number of annotated transcripts that were identified as differentially expressed, see Table 2. B) Hierarchical clustering of the whole transcriptome of the *Igf1*$^{-/-}$ *and Igf1*$^{+/+}$ vestibular organ per column (conditions). The similarity of gene expression between E18.5, P15 and P90 samples is represented by the vertical distances on each branch of the dendrogram. Gene expression is highly differentiated between embryonic and postnatal stages (E18.5 vs P15 and P90), but postnatal gene expressions are more correlated between genotypes than ages. Color bar describes each age: E18.5 (yellow), P15 (green) P90 (red) with different color shades *Igf1*$^{-/-}$ (dark) and *Igf1*$^{+/+}$ (light) according to the genotypes.

3.3. *Validation of differentially-expressed genes in the Igf1*$^{-/-}$ *mouse vestibule*

For the validation of the results obtained, the expression of three miRs and eight genes were analysed by RT-qPCR using TaqMan probes (Fig. 9). Table 3 shows the criteria for selecting the genes that included expression in the inner ear, association with inner ear diseases and differential expression in the array study at the time points studied. Among others *miR-181*, implicated in proliferation (Zhang et al., 2013), has previously been found to be down-regulated in the cochlea during ageing. The variations observed were confirmed in 53% of the genes studied by RT-qPCR analysis. At E18.5 the selected miRNAs (*miR-18*, *miR-148a* and *miR-181a-1*) showed a reduced transcript expression in the vestibule of *Igf1*$^{-/-}$ mice. In the case of *miR-18*, the expression in the *Igf1*$^{-/-}$ mouse was also decreased at P15 but increased at P90 when compared to that of the wild type mouse. *Mitf* transcripts were significantly decreased at E18.5, whereas the expression of *Ttr* significantly decreased at P15 and then it recovered control values at P90 (Fig. 9). At P15, *Pde1c* and *Enpp2* were differentially modulated in the *Igf1*$^{-/-}$ mouse vestibule, being increased and decreased, respectively, when compared to *Igf1*$^{+/+}$ mouse expression. CIDE-A belongs to a family of cell death activators encoded by the gene *Cidea* (Inohara et al., 1998) whose expression levels did not varied significantly along the ages and genotypes studied (data not shown). It promotes cell death and it is also a co-activator of the C/EBPβ transcription to regulate the expression of genes involved in immune and inflammatory responses, including pro-inflammatory cytokines and *Igf1* (Wang et al., 2012). The array analysis showed an increased expression of the genes *Dnajc5b* and *Grxcr1* in the *Igf1*$^{-/-}$ mouse vestibule at P90, but in the subsequent RT-qPCR study the increase was not significant. Both genes are expressed in the sensory neuroepithelia in the inner ear with

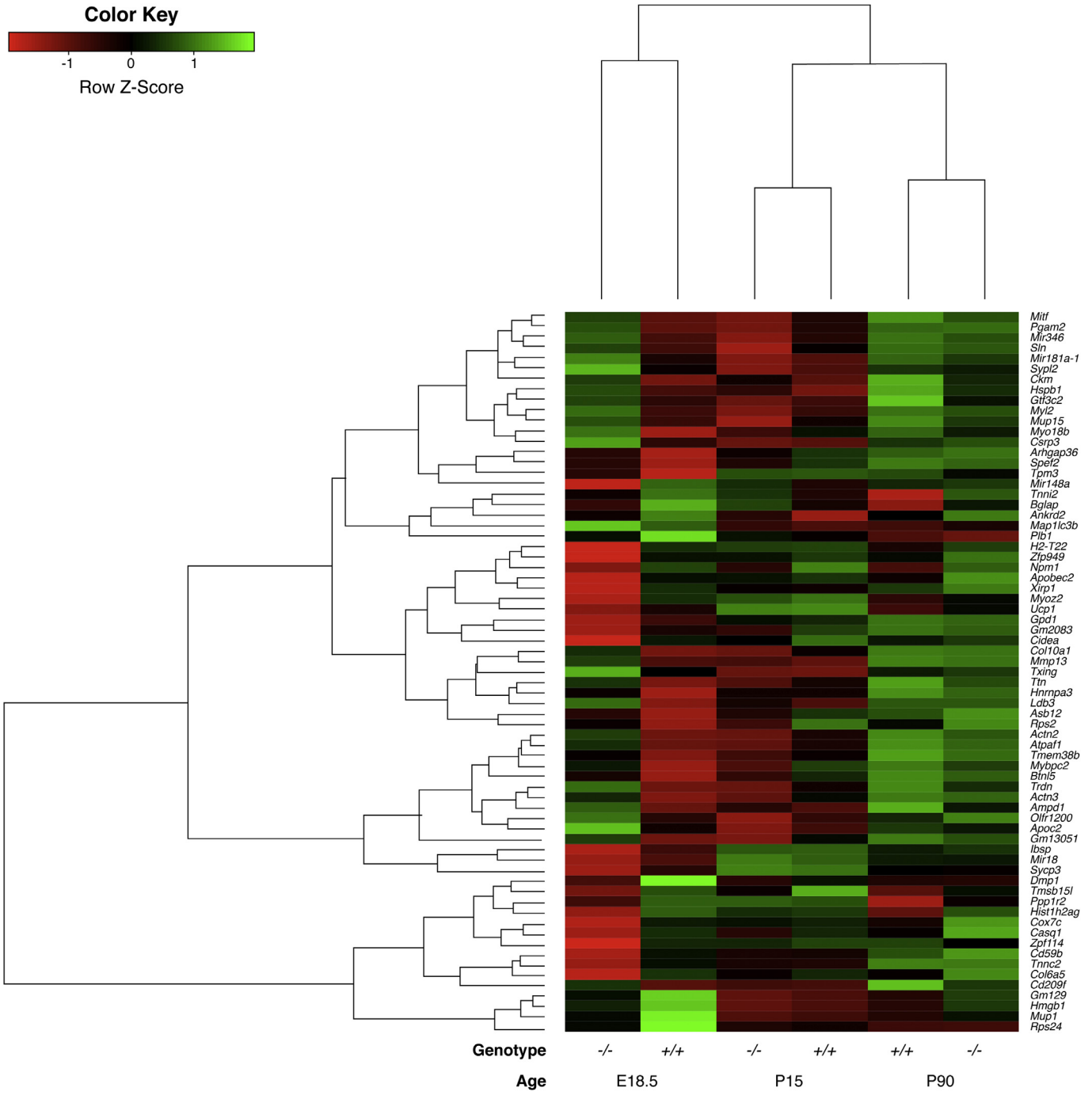

Fig. 5. Hierarchical clustering of E18.5 array data. Heatmap representing the hierarchical clustering of the Z scores of the differently expressed genes, when compared *Igf1*$^{-/-}$ *and* *Igf1*$^{+/+}$ mice at embryonic stage E18.5. The Z scores represent the dispersion around the overall mean of the gene expressions and weighted by their standard errors. The scale of the intensity is shown in the top corner. Correspondent values of the same genes at postnatal stages P15 and P90 are also shown.

highly restricted expression patterns, *Dnajc5b* is expressed in inner hair cells of adult mouse cochleae (Liu et al., 2014), whereas *Grxcr1* is localised in hair cell stereocilia of early postnatal mice (Odeh et al., 2010). Table 4 shows reported gene expression patterns of a subgroup of differentially expressed genes including the potassium channels *Kcne2* and *Kcnma1* and several transcription factors including *Pou1f1* and *Gtf3c2* (Visel et al., 2004; Beisel et al., 2007; Fang et al., 2012; Kurt et al., 2012).

4. Discussion

Transcriptome analysis of the vestibular organ showed striking differences between prenatal and postnatal ages in wild type mice, and significant gene expression differences with postnatal IGF-1 deficient mouse vestibules.

The *Igf1*$^{-/-}$ mouse did not show a vestibular phenotype in primary behavioral tests nor gross morphological differences with the vestibule of the wild type mouse. IGF-1 deficiency

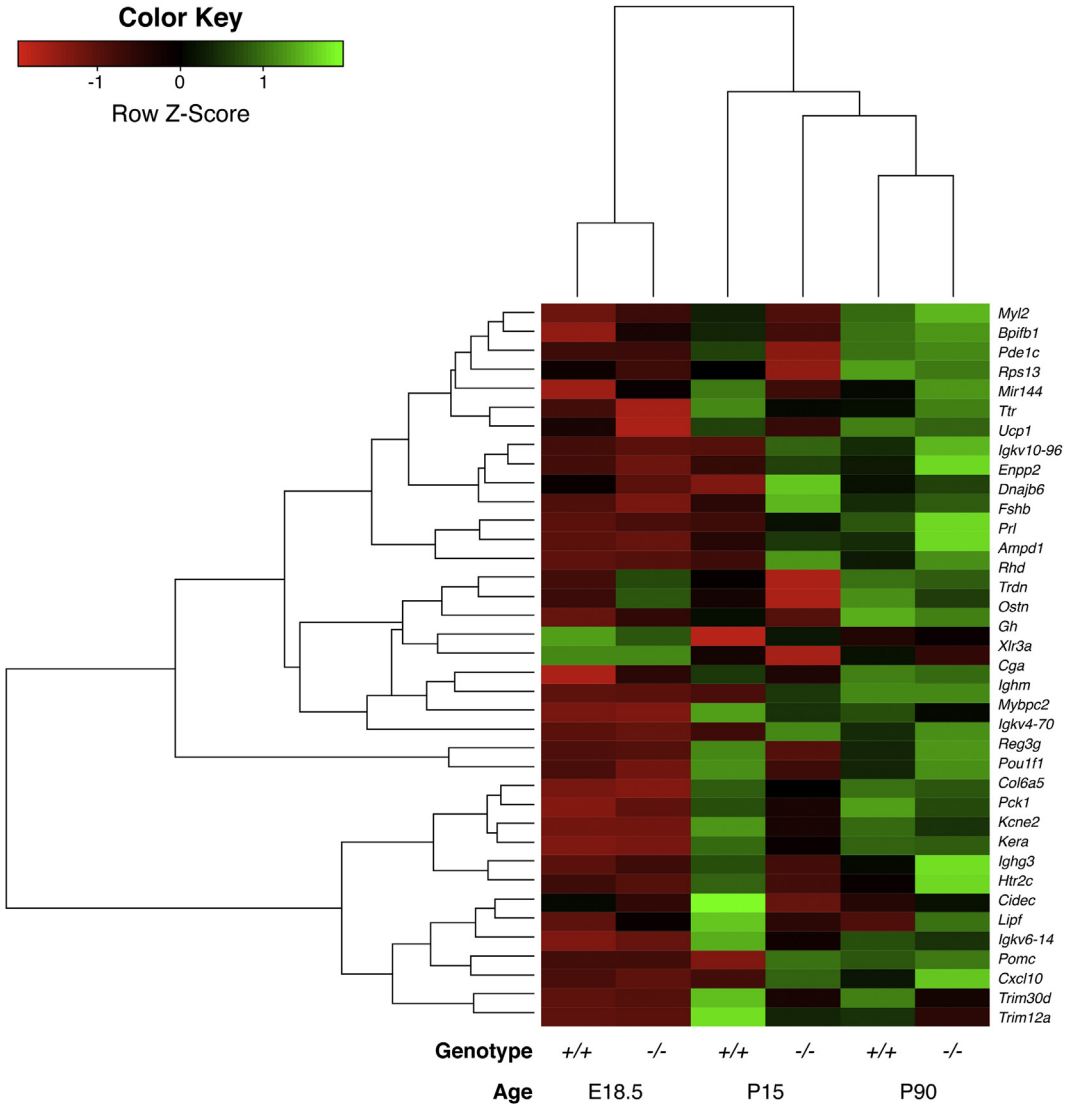

Fig. 6. Hierarchical clustering of P15 array data. Heatmap representing the hierarchical clustering of the Z scores of the differently expressed genes, when compared *Igf1*$^{-/-}$ *and* *Igf1*$^{+/+}$ mice at postnatal stage P15. The Z scores represent the dispersion around the overall mean of the gene expressions and weighted by their standard errors. The scale of the intensity is shown in the top corner. Correspondent values of the same targets at postnatal stages E18.5 and P90 are also shown.

differentially affects organ size (Rodriguez-De La Rosa et al., 2014). In this study we showed that the inner ear global size slightly decreased, this is also been previously reported (Riquelme et al., 2010). Embryonic IGF-1 deficit is compensated in the inner ear by IGF1R and by other insulin family members, but this compensation does not occur after birth (Sanchez-Calderon et al., 2010). IGF1R deficiency, in contrast, severely affects the development of the cochlea and the formation of the semicircular canals (Okano et al., 2011). Here we show that the absence of IGF-1 impairs the normal cellular postnatal development of the vestibular ganglion in mice. Parallel effects were reported in cochlear components of the inner ear, including the spiral ganglion (Camarero et al., 2001), but there are some differences. As a whole, the vestibular ganglion almost doubles in size between P5 and P20 in both *Igf1*$^{-/-}$ mice and their normal littermates, whereas the spiral ganglion does not change in size during the same age window in wild type mice, but has about 20% less of its volume in null mice at P20 (Camarero et al., 2001). Neuron numbers remained stable between P5 and P20 in the spiral ganglion, but showed an intriguing increase in the vestibular ganglion. It has been reported that new neurons are incorporated into postnatal and even adult peripheral dorsal root and trigeminal sensory ganglia in vertebrates, including rodents. However, it is debated whether they arise from division, maturation or migration of undifferentiated precursors (Farel, 2002; Lagares et al., 2007). Schwann cells have been recently proposed as a source of postnatal neurons in the enteric nervous system (Uesaka et al., 2015). No similar studies have been conducted in the vestibular ganglion and the data we collected in this study does not allow speculating further on this issue. However, such increase in neuron number seems to be dependent upon the presence of normal expression of IGF-1, since it only reached a statistical significance in wild type mice. Although the number of vestibular sensory neurons did not differ between genotypes at P5, their perikaryal size was already significantly smaller in *Igf1*$^{-/-}$ mice, suggesting that these effects appear earlier in the vestibular than the spiral ganglion, in which similar effects are overt at P20, but not P5 (Camarero et al., 2001). Cell size reduction has been reported for a number of cell types in

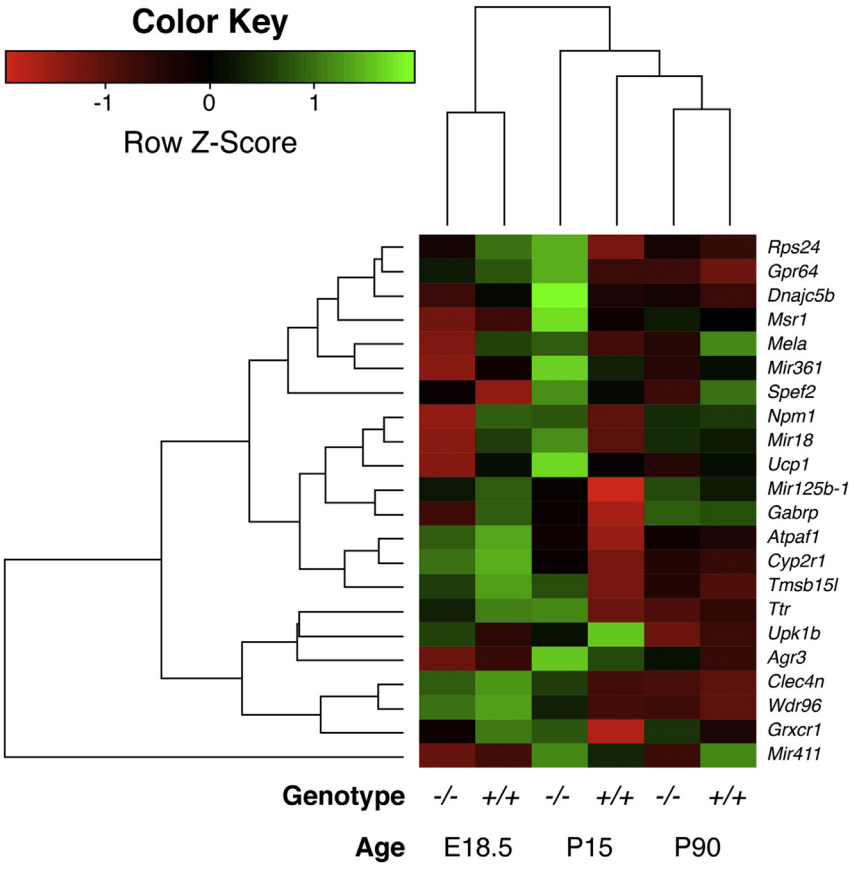

Fig. 7. Hierarchical clustering of P90 array data. Heatmap representing the hierarchical clustering of the Z scores of the differently expressed genes, when compared *Igf1*$^{-/-}$ *and* *Igf1*$^{+/+}$ mice at postnatal stage P90. The Z scores represent the dispersion around the overall mean of the gene expressions and weighted by their standard errors. The scale of the intensity is shown in the top corner. Correspondent values of the same targets at postnatal stages E18.5 and P15 are also shown.

different tissues, including the spiral ganglion, in *Igf1*$^{-/-}$ mice (Camarero et al., 2001; Rodriguez-de la Rosa et al., 2014).

Next we conducted the analysis of the transcriptome of the wild type and *Igf1*$^{-/-}$ mice vestibule at different stages of development, from embryonic age E18.5 to postnatal stages P15 and P90. With these transcriptomic profiles, we were able to perform comparative gene expression analysis of the vestibular organ across those development stages. We were able to show that the lack of IGF-1 in the vestibule alters the expression profiles of several genes that are also found expressed in the inner ear. The complexity of transcriptome and low levels of genes expression expected, were managed in this study by comparing results from different statistical methods and finally using a probabilistic approach to enable high accuracy in the detection of false positives. The sensitivity of the estimates from the whole transcript arrays revealed also interesting posttranscriptional effects in the alteration of the expression patterns of several miRs. More than 500 miRs have been so far described in the mammalian genome, each one is estimated to regulate up to 200 distinct target genes (Lim et al., 2005), highlighting their important role as post-transcriptional regulators of gene expression. Previous work had identified the expression and role of miRs in inner ear development function and disease (Lewis et al., 2009; Elkan-Miller et al., 2011; Patel et al., 2013; Ushakov et al., 2013; Bhonker et al., 2014). Targeted-IGF-1 miRs seem to be organ specific and essential for IGF-1 pro-survival and anti-inflammatory actions (Pelosi et al., 2015). *miR-18* and *miR-181* had been reported to be expressed in the inner ear, in this study we identified *miR-125b-1*, *miR-144*, *miR-148a*, *miR-346*, *miR-361* and *miR-411* as expressed in the vestibular organ and show a distinct time and/or genotype dependent expression pattern. *miR-18* is expressed in the cochlear spiral ganglion neurons and in hair cells and supporting cells of the vestibular sensory epithelium in newborn wild type mouse. *miR-18a* plays a key role in zebrafish inner ear development and morphogenesis (Friedman et al., 2009). *miR-181* is highly expressed in cochlear and vestibular epithelium of P0 C57Bl/6J mice (Rudnicki et al., 2014) and it is reported to play a key role in hair cell regeneration in explants of chicken auditory epithelia (Frucht et al., 2011). It expression was reported to be down-regulated in cochlea during ageing (Zhang et al., 2013). In the retina, *miR-181a/b* has been recently shown to master retinal axon specification and growth by modulating MAPK/ERK signaling and cytoskeletal rearrangement (Carrella et al., 2015). In this connection, the integrin signaling pathway is the most differentially expressed one at E18.5 among genotypes. Integrins are a family of cell surface receptors that play the role of integrating the interactions between the intracellular cytoskeleton with extracellular matrix proteins to modulate biological processes (Schwartz and Ginsberg, 2002). Signalling from integrins cooperate with those from growth factor receptors to organize the cytoskeleton, stimulate cell proliferation, growth, differentiation, migration, inflammatory responses, platelet aggregation, tissue repair and tumor invasion, rescue cells from matrix detachment and induced programmed cell death (Kumar, 1998;

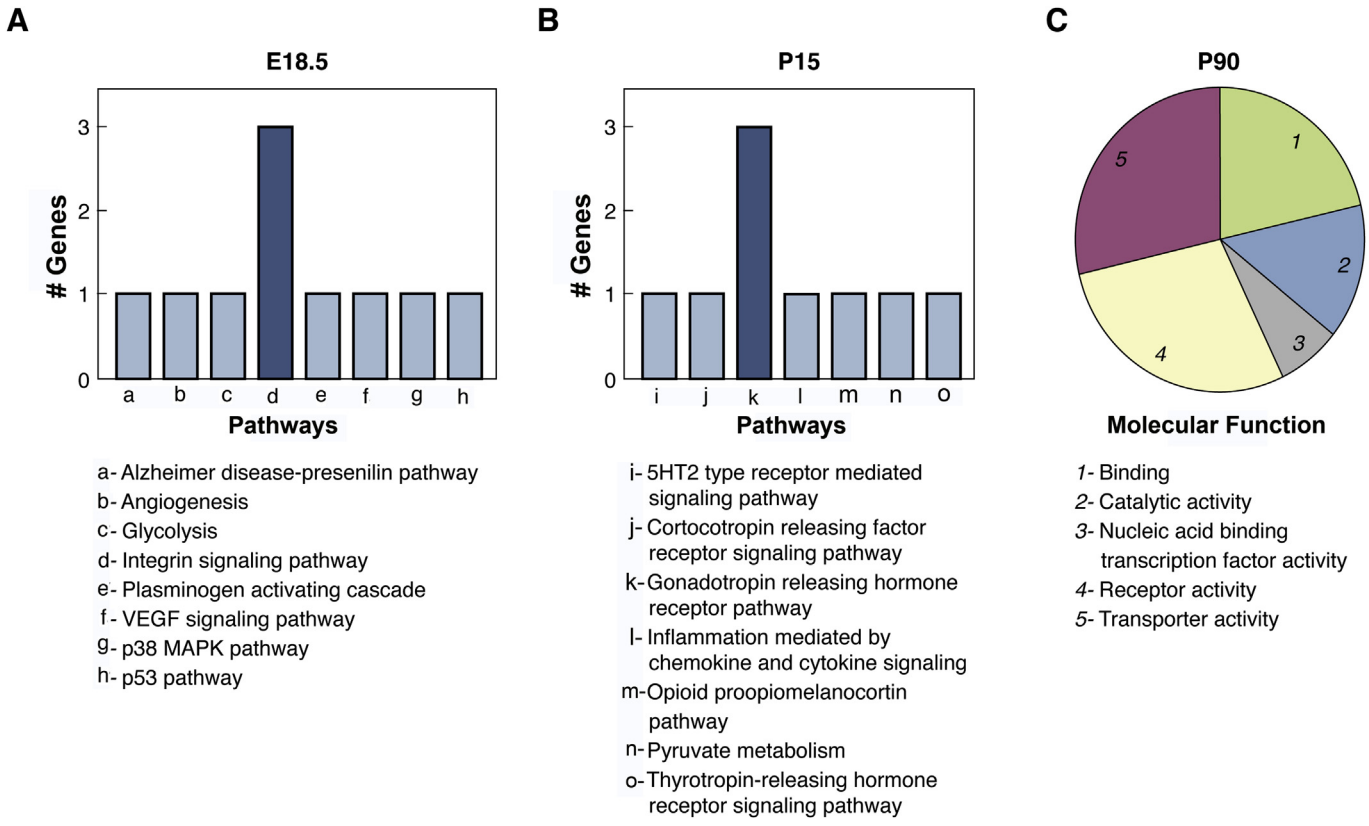

Fig. 8. Functional analysis of differentially expressed transcripts of *Igf1*$^{-/-}$ *and Igf1*$^{+/+}$ mice using PANTHER. Genes were categorised according to enriched pathways (A, B) and molecular functions (C). The analysis was conducted with PANTHER (http://www.pantherdb.org/). In A and B the pathways were selected as significant with p-value<0.05 obtained using PANTHER statistical and scoring tools. In C molecular functions were selected as per PANTHER enrichment tools. The number of genes from the differentially expressed list, associated to each enriched pathway or molecular function group is defined by the y-axix. Details of pathway components and genes associated to the selected molecular function groups are described in supplementary tables: Table S4, Table S5 and Table S6.

Martin et al., 2002; Schwartz and Ginsberg, 2002). *miR-148a* was reported previously to promote apoptosis (Zhang et al., 2011), to inhibit cell proliferation and tumor angiogenesis through targeting IGF1R and IRS1 and inhibiting AKT and ERK signaling pathways in breast cancer cell lines (Xu et al., 2013). In our analysis we also identified differentially expressed genes that include several associated with neurodegeneration, hearing loss and balance disorders. For example, mutations in the human transthyretin gene (*TTR*) cause hereditary amyloidosis and hearing loss (Klein et al., 1998; Brett et al., 1999), and microphthalmia-associated transcription factor (*Mitf*) mutations have been related to Waardenburg syndrome type 2, an auditory-pigmentary syndrome, where hypopigmentation and hearing loss are caused by the lack of melanocytes in skin and inner ear (Shibahara et al., 2001). Finally, autotaxin, also known as ectonucleotide pyrophosphatase/phosphodiesterase 2 (*Enpp2*) (Kawagoe et al., 1995), is a secreted enzyme that has lysophospholipase D activity and generates the lipid signaling molecule lysophosphatidic acid from lysophosphatidylcholine. Its functions are related with the stimulation of cell proliferation and chemotaxis, it also has angiogenic properties.

Accordingly, pathways affected in the developing and adult *Igf1*$^{-/-}$ mouse vestibule include those involved in stress and inflammatory responses (p38 MAPK and chemokine/cytokine signaling; corticotrophin-releasing hormone), angiogenesis (*Enpp2* and vascular endothelial growth factor) (Kawagoe et al., 1995), proteostasis (presenilin pathway, *Ttr*), neurohormone signalling (gonadotropin-releasing hormone, thyrotropin-releasing hormone and pro-opiomelanocortin) and DNA repair (p53) (Lopez-Otin et al., 2013). Neurotransmission (5HT2 serotonin receptors) (Hoyer et al., 1994) and glucose metabolism (glycolysis and pyruvate metabolism) were also differentially affected. Interestingly the *Igf1*$^{-/-}$ mouse cochlea also showed an undifferentiated and pro-inflammatory situation related to the p38 MAPK pathway (Sanchez-Calderon et al., 2010). It is important to note that here we present data obtained from the analysis of the whole vestibular organ, including non-sensory cells. Future work aims to compare these datasets with those obtained from the study of sensory cells, isolated as reported in (Oshima et al., 2007), to assess if *Igf1* deficiency has more impact on the development of sensory versus non-sensory vestibular cells.

In summary, here we offer additional insight into the pathophysiology of vestibular disorders and open new perspectives for the development of novel pharmacological strategies for their treatment.

5. Conclusions

We report here a comparative analysis of the gene expression profiles of postnatal and adult vestibular organs of wild type and IGF-1 deficient mice. We observed no striking functional and cellular alterations in the *Igf1*$^{-/-}$ mice but the transcriptome analysis revealed differences that may explain phenotypic differences in the vestibular neurons. The reported data contributes to identify novel miRs involved in the regulation of vestibular maturation including *miR-18*, *-125b-1*, *-144*, *-148a*, *-181a-1*, *-346*, *-361* and *-411*.

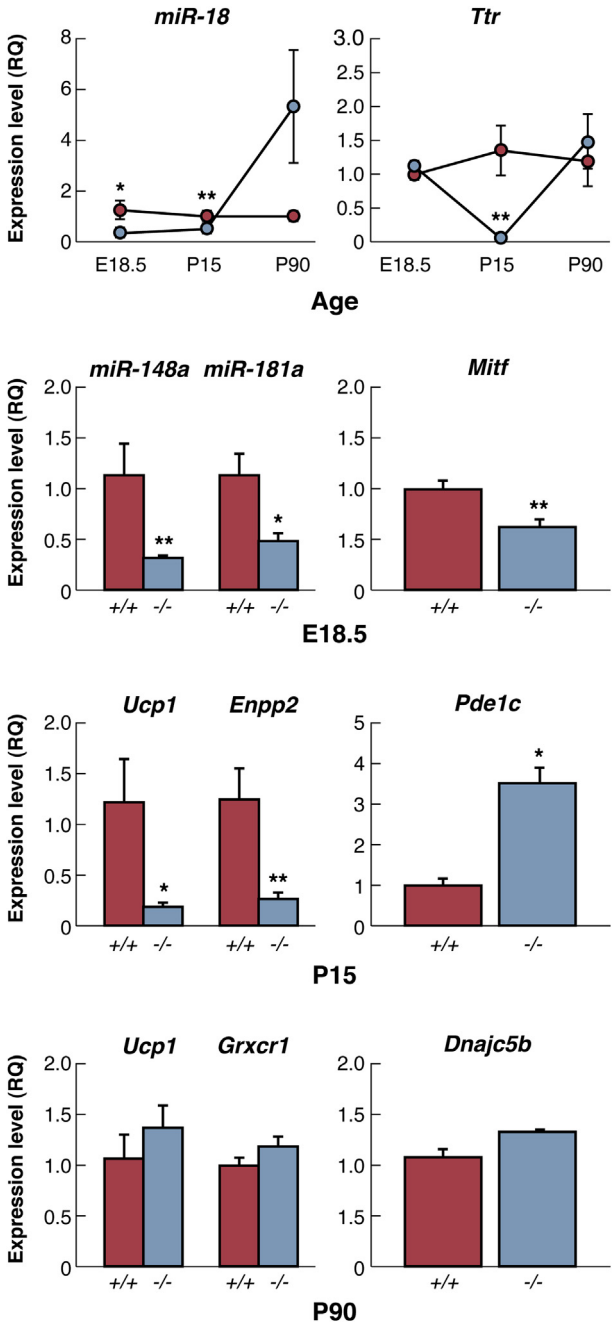

Fig. 9. Array data validation by RT-qPCR. miRNAs and gene expression levels of miR-18, miR-148a, miR-181a-1, Ttr, Ucp1, Mitf, Cidea, Enpp2, Pde1c, Dnajc5b and Grxcr1 were determined by RT-qPCR in the vestibular organs of *lgf1*$^{-/-}$ (black) and *lgf1*$^{+/+}$ (white) mice at different time points (E18.5, P15, P90). Data correspond to three samples, each prepared from pooling cochleae from two mice (6 mice in total). Rplp0 expression levels were used as endogenous housekeeping control gene, and the estimated expression was calculated as RQ ($2^{-\Delta\Delta Ct}$). Significant differences among animal groups are indicated by asterisks (*$p < 0.05$; **$p < 0.01$).

Acknowledgements

This study was supported by grants from FP7-PEOPLE-2013-IAPP 612261-TARGEAR to IVN, and CIBERER-INTRA/09/761.2 to IVN and JD. We thank Begoña Rodriguez for expert technical assistance with the celloidin material. LR-dlR and SM-C hold CIBERER contracts.

Appendix A. Supplementary data

Supplementary data related to this article can be found at http://dx.doi.org/10.1016/j.heares.2015.08.016.

References

Abe, S., Katagiri, T., Saito-Hisaminato, A., Usami, S., Inoue, Y., Tsunoda, T., Nakamura, Y., 2003. Identification of CRYM as a candidate responsible for nonsyndromic deafness, through cDNA microarray analysis of human cochlear and vestibular tissues. Am. J. Hum. Genet. 72, 73–82.

Aburto, M.R., Magarinos, M., Leon, Y., Varela-Nieto, I., Sanchez-Calderon, H., 2012. AKT signaling mediates IGF-I survival actions on otic neural progenitors. PLoS One 7, e30790. http://dx.doi.org/10.1371/journal.pone.0030790.

Angunsri, N., Taura, A., Nakagawa, T., Hayashi, Y., Kitajiri, S., Omi, E., Ishikawa, K., Ito, J., 2011. Insulin-like growth factor 1 protects vestibular hair cells from aminoglycosides. Neuroreport 22, 38–43. http://dx.doi.org/10.1097/WNR.0b013e32834273e9.

Banyard, J., Barrows, C., Zetter, B.R., 2009. Differential regulation of human thymosin beta 15 isoforms by transforming growth factor beta 1. Genes Chromosomes Cancer 48, 502–509. http://dx.doi.org/10.1002/gcc.20659.

Beisel, K.W., Rocha-Sanchez, S.M., Ziegenbein, S.J., Morris, K.A., Kai, C., Kawai, J., Carninci, P., Hayashizaki, Y., Davis, R.L., 2007. Diversity of Ca2+-activated K+ channel transcripts in inner ear hair cells. Gene 386, 11–23. http://dx.doi.org/10.1016/j.gene.2006.07.023.

Bhonker, Y., Ushakov, K., Avraham, K.B., 2014. Human gene discovery for understanding development of the inner ear and hearing loss. In: Romand, R., Varela-Nieto, I. (Eds.), Development of the Auditory and Vestibular Systems. Elsevier, pp. 107–127.

Bissonnette, J.P., Fekete, D.M., 1996. Standard atlas of the gross anatomy of the developing inner ear of the chicken. J. Comp. Neurol. 368, 620–630. http://dx.doi.org/10.1002/(SICI)1096-9861(19960513)368:4<620::AID-CNE12>3.0.CO;2-L.

Brett, M., Persey, M.R., Reilly, M.M., Revesz, T., Booth, D.R., Booth, S.E., Hawkins, P.N., Pepys, M.B., Morgan-Hughes, J.A., 1999. Transthyretin Leu12Pro is associated with systemic, neuropathic and leptomeningeal amyloidosis. Brain 122 (Pt 2), 183–190.

Camarero, G., Avendano, C., Fernandez-Moreno, C., Villar, A., Contreras, J., De Pablo, F., Pichel, J.G., Varela-Nieto, I., 2001. Delayed inner ear maturation and neuronal loss in postnatal Igf-1-deficient mice. J. Neurosci. 21, 7630–7641.

Camarero, G., Villar, M.A., Contreras, J., Fernandez-Moreno, C., Pichel, J.G., Avendano, C., Varela-Nieto, I., 2002. Cochlear abnormalities in insulin-like growth factor-1 mouse mutants. Hear Res. 170, 2–11.

Carrella, S., D'agostino, Y., Barbato, S., Huber-Reggi, S.P., Salierno, F.G., Manfredi, A., Neuhauss, S.C., Banfi, S., Conte, I., 2015. miR-181a/b control the assembly of visual circuitry by regulating retinal axon specification and growth. Dev. Neurobiol. http://dx.doi.org/10.1002/dneu.22282.

Cediel, R., Riquelme, R., Contreras, J., Diaz, A., Varela-Nieto, I., 2006. Sensorineural hearing loss in insulin-like growth factor I-null mice: a new model of human deafness. Eur. J. Neurosci. 23, 587–590. http://dx.doi.org/10.1111/j.1460-9568.2005.04584.x.

Chankiewitz, V., Morosan-Puopolo, G., Yusuf, F., Rudloff, S., Prols, F., Kleff, V., Hofmann, D.K., Brand-Saberi, B., 2014. A thymosin beta15-like peptide promotes intersegmental myotome extension in the chicken embryo, Histochem. Cell Biol. 141, 275–287. http://dx.doi.org/10.1007/s00418-013-1156-z.

Cruz-Orive, L.M., 1999. Precision of Cavalieri sections and slices with local errors. J. Microsc. 193, 182–198.

Degerman, E., Rauch, U., Lindberg, S., Caye-Thomasen, P., Hultgardh, A., Magnusson, M., 2013. Expression of insulin signalling components in the sensory epithelium of the human saccule. Cell Tissue Res. 352, 469–478. http://dx.doi.org/10.1007/s00441-013-1614-x.

Diez-Roux, G., Banfi, S., Sultan, M., Geffers, L., Anand, S., Rozado, D., Magen, A., Canidio, E., Pagani, M., Peluso, I., Lin-Marq, N., Koch, M., Bilio, M., Cantiello, I., Verde, R., De Masi, C., Bianchi, S.A., Cicchini, J., Perroud, E., Mehmeti, S., Dagand, E., Schrinner, S., Nurnberger, A., Schmidt, K., Metz, K., Zwingmann, C., Brieske, N., Springer, C., Hernandez, A.M., Herzog, S., Grabbe, F., Sieverding, C., Fischer, B., Schrader, K., Brockmeyer, M., Dettmer, S., Helbig, C., Alunni, V., Battaini, M.A., Mura, C., Henrichsen, C.N., Garcia-Lopez, R., Echevarria, D., Puelles, E., Garcia-Calero, E., Kruse, S., Uhr, M., Kauck, C., Feng, G., Milyaev, N., Ong, C.K., Kumar, L., Lam, M., Semple, C.A., Gyenesei, A., Mundlos, S., Radelof, U., Lehrach, H., Sarmientos, P., Reymond, A., Davidson, D.R., Dolle, P., Antonarakis, S.E., Yaspo, M.L., Martinez, S., Baldock, R.A., Eichele, G., Ballabio, A., 2011. A high-resolution anatomical atlas of the transcriptome in the mouse embryo. PLoS Biol. 9, e1000582. http://dx.doi.org/10.1371/journal.pbio.1000582.

Elkan-Miller, T., Ulitsky, I., Hertzano, R., Rudnicki, A., Dror, A.A., Lenz, D.R., Elkon, R., Irmler, M., Beckers, J., Shamir, R., Avraham, K.B., 2011. Integration of transcriptomics, proteomics, and microRNA analyses reveals novel microRNA regulation of targets in the mammalian inner ear. PLoS One 6, e18195. http://dx.doi.org/10.1371/journal.pone.0018195.

Fang, Q., Giordimaina, A.M., Dolan, D.F., Camper, S.A., Mustapha, M., 2012. Genetic background of Prop1(df) mutants provides remarkable protection against hypothyroidism-induced hearing impairment. J. Assoc. Res. Otolaryngol. 13, 173–184. http://dx.doi.org/10.1007/s10162-011-0302-3.

Farel, P.B., 2002. Sensory neuron addition in juvenile rat: time course and specificity. J. Comp. Neurol. 449, 158–165. http://dx.doi.org/10.1002/cne.10274.
Freeman, S., Priner, R., Mager, M., Sichel, J.Y., Perez, R., Elidan, J., Sohmer, H., 2000. Use of evoked potentials to objectively differentiate between selective vulnerability of cochlear and vestibular end organ function. J. Basic Clin. Physiol. Pharmacol. 11, 193–200.
Friedman, L.M., Dror, A.A., Mor, E., Tenne, T., Toren, G., Satoh, T., Biesemeier, D.J., Shomron, N., Fekete, D.M., Hornstein, E., Avraham, K.B., 2009. MicroRNAs are essential for development and function of inner ear hair cells in vertebrates. Proc. Natl. Acad. Sci. U. S. A. 106, 7915–7920. http://dx.doi.org/10.1073/pnas.0812446106.
Fritzsch, B., Pan, N., Jahan, I., Duncan, J.S., Kopecky, B.J., Elliott, K.L., Kersigo, J., Yang, T., 2013. Evolution and development of the tetrapod auditory system: an organ of Corti-centric perspective. Evol. Dev. 15, 63–79. http://dx.doi.org/10.1111/ede.12015.
Frucht, C.S., Santos-Sacchi, J., Navaratnam, D.S., 2011. MicroRNA181a plays a key role in hair cell regeneration in the avian auditory epithelium. Neurosci. Lett. 493, 44–48. http://dx.doi.org/10.1016/j.neulet.2011.02.017.
Fuentes-Santamaria, V., Alvarado, J.C., Rodriguez-De La Rosa, L., Murillo-Cuesta, S., Contreras, J., Juiz, J.M., Varela-Nieto, I., 2014. IGF-1 deficiency causes atrophic changes associated with upregulation of VGluT1 and downregulation of MEF2 transcription factors in the mouse cochlear nuclei. Brain Struct. Funct. http://dx.doi.org/10.1007/s00429-014-0934-2.
Gohma, H., Kuramoto, T., Kuwamura, M., Okajima, R., Tanimoto, N., Yamasaki, K., Nakanishi, S., Kitada, K., Makiyama, T., Akao, M., Kita, T., Sasa, M., Serikawa, T., 2006. WTC deafness Kyoto (dfk): a rat model for extensive investigations of Kcnq1 functions. Physiol. Genomics 24, 198–206. http://dx.doi.org/10.1152/physiolgenomics.00221.2005.
Gray, P.A., Fu, H., Luo, P., Zhao, Q., Yu, J., Ferrari, A., Tenzen, T., Yuk, D.I., Tsung, E.F., Cai, Z., Alberta, J.A., Cheng, L.P., Liu, Y., Stenman, J.M., Valerius, M.T., Billings, N., Kim, H.A., Greenberg, M.E., Mcmahon, A.P., Rowitch, D.H., Stiles, C.D., Ma, Q., 2004. Mouse brain organization revealed through direct genome-scale TF expression analysis. Science 306, 2255–2257. http://dx.doi.org/10.1126/science.1104935.
Gundersen, H.J., Bendtsen, T.F., Korbo, L., Marcussen, N., Moller, A., Nielsen, K., Nyengaard, J.R., Pakkenberg, B., Sorensen, F.B., Vesterby, A., et al., 1988. Some new, simple and efficient stereological methods and their use in pathological research and diagnosis. APMIS 96, 379–394.
Hardisty-Hughes, R.E., Parker, A., Brown, S.D., 2010. A hearing and vestibular phenotyping pipeline to identify mouse mutants with hearing impairment. Nat. Protoc. 5, 177–190. http://dx.doi.org/10.1038/nprot.2009.204.
Hertzano, R., Elkon, R., Kurima, K., Morrisson, A., Chan, S.L., Sallin, M., Biedlingmaier, A., Darling, D.S., Griffith, A.J., Eisenman, D.J., Strome, S.E., 2011. Cell type-specific transcriptome analysis reveals a major role for Zeb1 and miR-200b in mouse inner ear morphogenesis. PLoS Genet. 7, e1002309. http://dx.doi.org/10.1371/journal.pgen.1002309.
Hoyer, D., Clarke, D.E., Fozard, J.R., Hartig, P.R., Martin, G.R., Mylecharane, E.J., Saxena, P.R., Humphrey, P.P., 1994. International union of pharmacology classification of receptors for 5-hydroxytryptamine (Serotonin). Pharmacol. Rev. 46, 157–203.
Huang, M., Sage, C., Tang, Y., Lee, S.G., Petrillo, M., Hinds, P.W., Chen, Z.Y., 2011. Overlapping and distinct pRb pathways in the mammalian auditory and vestibular organs. Cell Cycle 10, 337–351.
Huber, W., Von Heydebreck, A., Sultmann, H., Poustka, A., Vingron, M., 2002. Variance stabilization applied to microarray data calibration and to the quantification of differential expression. Bioinformatics 18 (Suppl. 1), S96–S104.
Inohara, N., Koseki, T., Chen, S., Wu, X., Nunez, G., 1998. CIDE, a novel family of cell death activators with homology to the 45 kDa subunit of the DNA fragmentation factor. EMBO J. 17, 2526–2533. http://dx.doi.org/10.1093/emboj/17.9.2526.
Irizarry, R.A., Hobbs, B., Collin, F., Beazer-Barclay, Y.D., Antonellis, K.J., Scherf, U., Speed, T.P., 2003. Exploration, normalization, and summaries of high density oligonucleotide array probe level data. Biostatistics 4, 249–264. http://dx.doi.org/10.1093/biostatistics/4.2.249.
Kitahara, T., Li-Korotky, H.S., Balaban, C.D., 2005. Regulation of mitochondrial uncoupling proteins in mouse inner ear ganglion cells in response to systemic kanamycin challenge. Neuroscience 135, 639–653. http://dx.doi.org/10.1016/j.neuroscience.2005.06.056.
Kawagoe, H., Soma, O., Goji, J., Nishimura, N., Narita, M., Inazawa, J., Nakamura, H., Sano, K., 1995. Molecular cloning and chromosomal assignment of the human brain-type phosphodiesterase I/nucleotide pyrophosphatase gene (PDNP2). Genomics 30, 380–384. http://dx.doi.org/10.1006/geno.1995.0036.
Klein, C.J., Nakumura, M., Jacobson, D.R., Lacy, M.Q., Benson, M.D., Petersen, R.C., 1998. Transthyretin amyloidosis (serine 44) with headache, hearing loss, and peripheral neuropathy. Neurology 51, 1462–1464.
Knox, G.W., Isaacs, J., Woodard, D., Johnson, L., Jordan, D., 1993. Short latency vestibular evoked potentials. Otolaryngol. Head. Neck Surg. 108, 265–269.
Kopke, R.D., Jackson, R.L., Li, G., Rasmussen, M.D., Hoffer, M.E., Frenz, D.A., Costello, M., Schultheiss, P., Van De Water, T.R., 2001. Growth factor treatment enhances vestibular hair cell renewal and results in improved vestibular function. Proc. Natl. Acad. Sci. U. S. A. 98, 5886–5891. http://dx.doi.org/10.1073/pnas.101120898.
Kuhn, S., Ingham, N., Pearson, S., Gribble, S.M., Clayton, S., Steel, K.P., Marcotti, W., 2012. Auditory function in the Tc1 mouse model of down syndrome suggests a limited region of human chromosome 21 involved in otitis media. PLoS One 7, e31433. http://dx.doi.org/10.1371/journal.pone.0031433.
Kumar, C.C., 1998. Signaling by integrin receptors. Oncogene 17, 1365–1373. http://dx.doi.org/10.1038/sj.onc.1202172.
Kurt, S., Sausbier, M., Ruttiger, L., Brandt, N., Moeller, C.K., Kindler, J., Sausbier, U., Zimmermann, U., Van Straaten, H., Neuhuber, W., Engel, J., Knipper, M., Ruth, P., Schulze, H., 2012. Critical role for cochlear hair cell BK channels for coding the temporal structure and dynamic range of auditory information for central auditory processing. FASEB J. 26, 3834–3843. http://dx.doi.org/10.1096/fj.11-200535.
Lagares, A., Li, H.Y., Zhou, X.F., Avendano, C., 2007. Primary sensory neuron addition in the adult rat trigeminal ganglion: evidence for neural crest glio-neuronal precursor maturation. J. Neurosci. 27, 7939–7953. http://dx.doi.org/10.1523/JNEUROSCI.1203-07.2007.
Ladrech, S., Mathieu, M., Puel, J.L., Lenoir, M., 2013. Supporting cells regulate the remodelling of aminoglycoside-injured organ of Corti, through the release of high mobility group box 1. Eur. J. Neurosci 38, 2962–2972. http://dx.doi.org/10.1111/ejn.12290.
Lewis, M.A., Quint, E., Glazier, A.M., Fuchs, H., De Angelis, M.H., Langford, C., Van Dongen, S., Abreu-Goodger, C., Piipari, M., Redshaw, N., Dalmay, T., Moreno-Pelayo, M.A., Enright, A.J., Steel, K.P., 2009. An ENU-induced mutation of miR-96 associated with progressive hearing loss in mice. Nat. Genet. 41, 614–618. http://dx.doi.org/10.1038/ng.369.
Lim, L.P., Lau, N.C., Garrett-Engele, P., Grimson, A., Schelter, J.M., Castle, J., Bartel, D.P., Linsley, P.S., Johnson, J.M., 2005. Microarray analysis shows that some microRNAs downregulate large numbers of target mRNAs. Nature 433, 769–773. http://dx.doi.org/10.1038/nature03315.
Liu, X., Newton, V., Read, A., 1995. Hearing loss and pigmentary disturbances in Waardenburg syndrome with reference to WS type II. J. Laryngol. Otol 109, 96–100.
Liu, H., Pecka, J.L., Zhang, Q., Soukup, G.A., Beisel, K.W., He, D.Z., 2014. Characterization of transcriptomes of cochlear inner and outer hair cells. J. Neurosci. 34, 11085–11095. http://dx.doi.org/10.1523/JNEUROSCI.1690-14.2014.
Liu, J.P., Baker, J., Perkins, A.S., Robertson, E.J., Efstratiadis, A., 1993. Mice carrying null mutations of the genes encoding insulin-like growth factor I (Igf-1) and type 1 IGF receptor (Igf1r). Cell 75, 59–72.
Lopez-Otin, C., Blasco, M.A., Partridge, L., Serrano, M., Kroemer, G., 2013. The hallmarks of aging. Cell 153, 1194–1217. http://dx.doi.org/10.1016/j.cell.2013.05.039.
Magarinos, M., Contreras, J., Aburto, M.R., Varela-Nieto, I., 2012. Early development of the vertebrate inner ear. Anat. Rec. Hob. 295, 1775–1790. http://dx.doi.org/10.1002/ar.22575.
Magarinos, M., Contreras, J., Varela-Nieto, I., 2014. Early development of the vertebrate inner ear. In: Romand, R., Varela-Nieto, I. (Eds.), Development of the Auditory and Vestibular Systems. Elsevier, pp. 1–30.
Maklad, A., Fritzsch, B., 2003. Development of vestibular afferent projections into the hindbrain and their central targets. Brain Res. Bull. 60, 497–510.
Martin, K.H., Slack, J.K., Boerner, S.A., Martin, C.C., Parsons, J.T., 2002. Integrin connections map: to infinity and beyond. Science 296, 1652–1653. http://dx.doi.org/10.1126/science.296.5573.1652.
Mi, H., Thomas, P., 2009. PANTHER pathway: an ontology-based pathway database coupled with data analysis tools. Methods Mol. Biol. 563, 123–140. http://dx.doi.org/10.1007/978-1-60761-175-2_7.
Mootha, V., Lindgren, C., Eriksson, K., Subramanian, A., , et al.Groop, L., 2003. PGC-1alpha-responsive genes involved in oxidative phosphorylation are coordinately downregulated in human diabetes. Nat. Genet. 34, 267–273.
Munoz-Espin, D., Canamero, M., Maraver, A., Gomez-Lopez, G., Contreras, J., Murillo-Cuesta, S., Rodriguez-Baeza, A., Varela-Nieto, I., Ruberte, J., Collado, M., Serrano, M., 2013. Programmed cell senescence during mammalian embryonic development. Cell 155, 1104–1118. http://dx.doi.org/10.1016/j.cell.2013.10.019.
Murillo-Cuesta, S., Camarero, G., Gonzalez-Rodriguez, A., De La Rosa, L.R., Burks, D.J., Avendano, C., Valverde, A.M., Varela-Nieto, I., 2012. Insulin receptor substrate 2 (IRS2)-deficient mice show sensorineural hearing loss that is delayed by concomitant protein tyrosine phosphatase 1B (PTP1B) loss of function. Mol. Med. 18, 260–269. http://dx.doi.org/10.2119/molmed.2011.00328.
Murillo-Cuesta, S., Rodriguez-De La Rosa, L., Cediel, R., Lassaletta, L., Varela-Nieto, I., 2011. The role of insulin-like growth factor-I in the physiopathology of hearing. Front. Mol. Neurosci. 4, 11. http://dx.doi.org/10.3389/fnmol.2011.00011.
Nakagawa, T., Ogino-Nishimura, E., Hiraumi, H., Sakamoto, T., Yamamoto, N., Ito, J., 2012. Audiometric outcomes of topical IGF1 treatment for sudden deafness refractory to systemic steroids. Otol. Neurotol. 33, 941–946. http://dx.doi.org/10.1097/MAO.0b013e31825f251a.
Odeh, H., Hunker, K.L., Belyantseva, I.A., Azaiez, H., Avenarius, M.R., Zheng, L., Peters, L.M., Gagnon, L.H., Hagiwara, N., Skynner, M.J., Brilliant, M.H., Allen, N.D., Riazuddin, S., Johnson, K.R., Raphael, Y., Najmabadi, H., Friedman, T.B., Bartles, J.R., Smith, R.J., Kohrman, D.C., 2010. Mutations in Grxcr1 are the basis for inner ear dysfunction in the pirouette mouse. Am. J. Hum. Genet. 86, 148–160. http://dx.doi.org/10.1016/j.ajhg.2010.01.016.
Okano, T., Kelley, M.W., 2013. Expression of insulin-like growth factor binding proteins during mouse cochlear development. Dev. Dyn. 242, 1210–1221. http://dx.doi.org/10.1002/dvdy.24005.
Okano, T., Xuan, S., Kelley, M.W., 2011. Insulin-like growth factor signaling regulates the timing of sensory cell differentiation in the mouse cochlea. J. Neurosci. 31, 18104–18118. http://dx.doi.org/10.1523/JNEUROSCI.3619-11.2011.
Oshima, K., Grimm, C.M., Corrales, C.E., Senn, P., Martinez Monedero, R., Géléoc, G.S.G., , et al.Heller, S., 2007. Differential distribution of stem cells in the auditory and vestibular organs of the inner ear. JARO J. Assoc. Res. Otolaryngol.

8 (1), 18–31. http://dx.doi.org/10.1007/s10162-006-0058-3.
Patel, M., Cai, Q., Ding, D., Salvi, R., Hu, Z., Hu, B.H., 2013. The miR-183/Taok1 target pair is implicated in cochlear responses to acoustic trauma. PLoS One 8, e58471. http://dx.doi.org/10.1371/journal.pone.0058471.
Pelosi, L., Coggi, A., Forcina, L., Musaro, A., 2015. MicroRNAs modulated by local mIGF-1 expression in mdx dystrophic mice. Front. Aging Neurosci. 7, 69. http://dx.doi.org/10.3389/fnagi.2015.00069.
Ruffell, D., Mourkioti, F., Gambardella, A., Kirstetter, P., Lopez, R.G., Rosenthal, N., Nerlov, C., 2009. A CREB-C/EBPbeta cascade induces M2 macrophage-specific gene expression and promotes muscle injury repair,. Proc. Natl. Acad. Sci. U S A 106, 17475–17480. http://dx.doi.org/10.1073/pnas.0908641106.
Riquelme, R., Cediel, R., Contreras, J., La Rosa Lourdes, R.D., Murillo-Cuesta, S., Hernandez-Sanchez, C., Zubeldia, J.M., Cerdan, S., Varela-Nieto, I., 2010. A comparative study of age-related hearing loss in wild type and insulin-like growth factor I deficient mice. Front. Neuroanat. 4, 27. http://dx.doi.org/10.3389/fnana.2010.00027.
Rodriguez-De La Rosa, L., Fernandez-Sanchez, L., Germain, F., Murillo-Cuesta, S., Varela-Nieto, I., De La Villa, P., Cuenca, N., 2012. Age-related functional and structural retinal modifications in the Igf1-/- null mouse. Neurobiol. Dis. 46, 476–485. http://dx.doi.org/10.1016/j.nbd.2012.02.013.
Rodriguez-De La Rosa, L., Lopez-Herradon, A., Portal-Nunez, S., Murillo-Cuesta, S., Lozano, D., Cediel, R., Varela-Nieto, I., Esbrit, P., 2014. Treatment with N- and C-terminal peptides of parathyroid hormone-related protein partly compensate the skeletal abnormalities in IGF-I deficient mice. PLoS One 9, e87536. http://dx.doi.org/10.1371/journal.pone.0087536.
Rudnicki, A., Isakov, O., Ushakov, K., Shivatzki, S., Weiss, I., Friedman, L.M., Shomron, N., Avraham, K.B., 2014. Next-generation sequencing of small RNAs from inner ear sensory epithelium identifies microRNAs and defines regulatory pathways. BMC Genomics 15, 484. http://dx.doi.org/10.1186/1471-2164-15-484.
Sanchez-Calderon, H., Milo, M., Leon, Y., Varela-Nieto, I., 2007. A network of growth and transcription factors controls neuronal differentation and survival in the developing ear. Int. J. Dev. Biol. 51, 557–570. http://dx.doi.org/10.1387/ijdb.072373hs.
Sanchez-Calderon, H., Rodriguez-De La Rosa, L., Milo, M., Pichel, J.G., Holley, M., Varela-Nieto, I., 2010. RNA microarray analysis in prenatal mouse cochlea reveals novel IGF-I target genes: implication of MEF2 and FOXM1 transcription factors. PLoS One 5, e8699. http://dx.doi.org/10.1371/journal.pone.0008699.
Schwartz, M.A., Ginsberg, M.H., 2002. Networks and crosstalk: integrin signalling spreads. Nat. Cell Biol. 4, E65–E68. http://dx.doi.org/10.1038/ncb0402-e65.
Schraders, M., Lee, K., Oostrik, J., Huygen, P.L., Ali, G., Hoefsloot, L.H., Veltman, J.A., Cremers, F.P., Basit, S., Ansar, M., Cremers, C.W., Kunst, H.P., Ahmad, W., Admiraal, R.J., Leal, S.M., Kremer, H., 2010. Homozygosity mapping reveals mutations of GRXCR1 as a cause of autosomal-recessive nonsyndromic hearing impairment. Am. J. Hum. Genet. 86, 138–147. http://dx.doi.org/10.1016/j.ajhg.2009.12.017.
Shibahara, S., Takeda, K., Yasumoto, K., Udono, T., Watanabe, K., Saito, H., Takahashi, K., 2001. Microphthalmia-associated transcription factor (MITF): multiplicity in structure, function, and regulation. J. Investig. Dermatol. Symp. Proc. 6, 99–104. http://dx.doi.org/10.1046/j.0022-202x.2001.00010.x.
Smith, S.D., Kelley, P.M., Kenyon, J.B., Hoover, D., 2000. Tietz syndrome (hypopigmentation/deafness) caused by mutation of MITF. J. Med. Genet. 37, 446–448.
Soto, E., Vega, R., Sesena, E., 2013. Neuropharmacological basis of vestibular system disorder treatment. J. Vestib. Res. 23, 119–137. http://dx.doi.org/10.3233/VES-130494.
Sausbier, M., Hu, H., Arntz, C., Feil, S., Kamm, S., Adelsberger, H., Sausbier, U., Sailer, C.A., Feil, R., Hofmann, F., Korth, M., Shipston, M.J., Knaus, H.G., Wolfer, D.P., Pedroarena, C.M., Storm, J.F., Ruth, P., 2004. Cerebellar ataxia and Purkinje cell dysfunction caused by Ca2+-activated K+ channel deficiency. Proc. Natl. Acad. Sci. U S A 101, 9474–9478. http://dx.doi.org/10.1073/pnas.0401702101.
Subramanian, A., Tamayo, P., Mootha, V., Mukherjee, S., Ebert, B., Gillette, M., Paulovich, A., Pomeroy, S., Golub, T., Lander, E., Mesirov, Jill P., 2005. Gene set enrichment analysis: a knowledge-based approach for interpreting genome-wide expression profiles. PNAS 2005 102 (43), 15545–15550.
Tafra, R., Brakus, S.M., Vukojevic, K., Kablar, B., Colovic, Z., Saraga-Babic, M., 2014. Interplay of proliferation and proapoptotic and antiapoptotic factors is revealed in the early human inner ear development. Otol. Neurotol. 35, 695–703. http://dx.doi.org/10.1097/MAO.0000000000000210.
Takeo, C., Ikeda, K., Horie-Inoue, K., Inoue, S., 2009. Identification of Igf2, Igfbp2 and Enpp2 as estrogen-responsive genes in rat hippocampus. Endocr. J. 56, 113–120.
Tandrup, T., Gundersen, H.J., Jensen, E.B., 1997. The optical rotator. J. Microsc. 186, 108–120.
Turro, E., Lewin, A., Rose, A., Dallman, M.J., Richardson, S., 2010. MMBGX: a method for estimating expression at the isoform level and detecting differential splicing using whole-transcript Affymetrix arrays. Nucleic Acids Res. 38, e4. http://dx.doi.org/10.1093/nar/gkp853.
Uesaka, T., Nagashimada, M., Enomoto, H., 2015. Neuronal differentiation in Schwann cell lineage underlies postnatal neurogenesis in the enteric nervous system. J. Neurosci. 35, 9879–9888. http://dx.doi.org/10.1523/JNEUROSCI.1239-15.2015.
Ushakov, K., Rudnicki, A., Avraham, K.B., 2013. MicroRNAs in sensorineural diseases of the ear. Front. Mol. Neurosci. 6, 52. http://dx.doi.org/10.3389/fnmol.2013.00052.
Varela-Nieto, I., Murillo-Cuesta, S., Rodriguez-De La Rosa, L., Lassatetta, L., Contreras, J., 2013. IGF-I deficiency and hearing loss: molecular clues and clinical implications. Pediatr. Endocrinol. Rev. 10, 460–472.
Visel, A., Thaller, C., Eichele, G., 2004. GenePaint.org: an atlas of gene expression patterns in the mouse embryo. Nucleic Acids Res. 32, D552–D556. http://dx.doi.org/10.1093/nar/gkh029.
Wang, W., Lv, N., Zhang, S., Shui, G., Qian, H., Zhang, J., Chen, Y., Ye, J., Xie, Y., Shen, Y., Wenk, M.R., Li, P., 2012. Cidea is an essential transcriptional coactivator regulating mammary gland secretion of milk lipids. Nat. Med. 18, 235–243. http://dx.doi.org/10.1038/nm.2614.
West, M.J., 1993. New stereological methods for counting neurons. Neurobiol. Aging 14, 275–285.
Xu, Q., Jiang, Y., Yin, Y., Li, Q., He, J., Jing, Y., Qi, Y.T., Xu, Q., Li, W., Lu, B., Peiper, S.S., Jiang, B.H., Liu, L.Z., 2013. A regulatory circuit of miR-148a/152 and DNMT1 in modulating cell transformation and tumor angiogenesis through IGF-IR and IRS1. J. Mol. Cell Biol. 5, 3–13. http://dx.doi.org/10.1093/jmcb/mjs049.
Yamamoto, N., Nakagawa, T., Ito, J., 2014. Application of insulin-like growth factor-1 in the treatment of inner ear disorders. Front. Pharmacol. 5, 208. http://dx.doi.org/10.3389/fphar.2014.00208.
Zhang, H., Li, Y., Huang, Q., Ren, X., Hu, H., Sheng, H., Lai, M., 2011. MiR-148a promotes apoptosis by targeting Bcl-2 in colorectal cancer. Cell Death Differ. 18, 1702–1710. http://dx.doi.org/10.1038/cdd.2011.28.
Zhang, Q., Liu, H., Mcgee, J., Walsh, E.J., Soukup, G.A., He, D.Z., 2013. Identifying microRNAs involved in degeneration of the organ of corti during age-related hearing loss. PLoS One 8, e62786. http://dx.doi.org/10.1371/journal.pone.0062786.